

Article

A Novel Adaptive Manta-Ray Foraging Optimization for Stochastic ORPD Considering Uncertainties of Wind Power and Load Demand

Sulaiman Z. Almutairi ^{1,*}, Emad A. Mohamed ^{1,2}  and Fayez F. M. El-Sousy ¹ 

¹ Department of Electrical Engineering, College of Engineering, Prince Sattam bin Abdulaziz University, Al Kharj 16278, Saudi Arabia; e.younis@psau.edu.sa (E.A.M.); f.elsousy@psau.edu.sa (F.F.M.E.-S.)

² Department of Electrical Engineering, Faculty of Engineering, Aswan University, Aswan 81542, Egypt

* Correspondence: s.almutairi@psau.edu.sa

Abstract: The optimal control of reactive powers in electrical systems can improve a system's performance and security; this can be provided by the optimal reactive power dispatch (ORPD). Under the high penetration of renewable energy resources (RERs) such as wind turbines (WTs), the ORPD problem solution has become a challenging and complex task due to the fluctuations and uncertainties of generated power from WTs. In this regard, this paper solved the conventional ORPD and the stochastic ORPD (SORPD) at uncertainties of the generated power from WTs and the load demand. An Adaptive Manta-Ray Foraging Optimization (AMRFO) was presented based on three modifications, including the fitness distance balance selection (FDB), Quasi Oppositional based learning (QOBL), and an adaptive Levy Flight (ALF). The ORPD and SORPD were solved to reduce the power loss (P_{Loss}) and the total expected P_{Loss} (TEPL), the voltage deviations (VD) and the total expected VD (TEVD). The normal and Weibull probability density functions (PDFs), along with the scenario reduction method and the Monte Carlo simulation (MCS), were utilized for uncertainty representations. The performance and validity of the suggested AMRFO were compared to other optimizers, including SCSO, WOA, DO, AHA, and the conventional MRFO on the IEEE 30-bus system and standard benchmark functions. These simulation results confirm the supremacy of the suggested AMRFO for the ORPD and SORPD solution compared to the other reported techniques.

Keywords: ORPD; wind power; uncertainty; optimization

MSC: 68N30



Citation: Almutairi, S.Z.; Mohamed, E.A.; El-Sousy, F.F.M. A Novel Adaptive Manta-Ray Foraging Optimization for Stochastic ORPD Considering Uncertainties of Wind Power and Load Demand.

Mathematics **2023**, *11*, 2591. <https://doi.org/10.3390/math11112591>

Academic Editor: Konstantin Kozlov

Received: 6 May 2023

Revised: 29 May 2023

Accepted: 1 June 2023

Published: 5 June 2023



Copyright: © 2023 by the authors. Licensee MDPI, Basel, Switzerland. This article is an open access article distributed under the terms and conditions of the Creative Commons Attribution (CC BY) license (<https://creativecommons.org/licenses/by/4.0/>).

1. Introduction

The ORPD problem solution is an important task that can play a vital role in improving the power system's performance, reliability and stability. The ORPD represents an optimal power flow (OPF) problem sub-problem that aims to assign the best values of the system control variables, such as the voltages of the generators, the transformer's taps and the Vars output of compensators while satisfying the operational constraints. In the ORPD solution, the voltage deviations, the power losses, and the system stability are optimized simultaneously or separately [1–3].

The ORPD is a nonlinear and complex problem where various classical methods can be utilized to solve this problem, such as an interior point method [4], the unified method [5], the linear programming approach [6], and the quadratic problem approach [7]. However, while these classical methods are robust in small power systems, they are difficult to apply to large-scale systems. Furthermore, these approaches suffer from stagnation. In this regard, meta-heuristic techniques were developed to optimize the ORPD. These meta-heuristic algorithms could be categorized as provided in Table 1. As listed in Table 1, the first meta-heuristic type was evolutionary-based techniques which mimic the evolution process

of creatures naturally, such as species migration and natural selection. The swarm-based techniques are nature-based algorithms that mimic the cooperative activities of animals within specific communities or swarms, such as flocks of birds and ant colonies. Physical-based techniques are efficient types of optimization algorithms that are conceptualized from the physical phenomena or laws of physics. Human-based techniques are optimization algorithms that are conceptualized with human behavior and thinking. The hybrid-based algorithms are algorithms that are based on the combination of two algorithms from the previous techniques. The main advantage of the listed optimization techniques in Table 1 is that these methods are simple to apply for solving the conventional ORPD, while the main shortage of these methods is that the uncertainties and the stochastic nature of the system, are not considered, including the uncertainties loading and output power of the renewable energy resources.

Table 1. Review of the applied algorithms for solving the ORPD.

Evolutionary-Based Techniques	Swarm-Based Techniques
<ul style="list-style-type: none"> ▪ Differential Evolution [8] ▪ Enhanced Grey Wolf Optimizer (EGWO) [10] ▪ Specialized Genetic Algorithm) [12] ▪ Pareto Evolutionary Algorithm [14] ▪ Modified Differential Evolution [16] ▪ Evolutionary Programming [2] ▪ Comprehensive Learning PSO [19] 	<ul style="list-style-type: none"> ▪ Particle Swarm Optimization (PSO) [9] ▪ Moth Swarm Algorithm [11] ▪ Improved Antlion Optimization technique [13] ▪ Improved Social Spider Optimization [15] ▪ Whale Optimization technique [17] ▪ Ant Lion Optimizer [18] ▪ Marine Predators Algorithm [20]
Physical-Based Techniques	Human-Based Techniques
<ul style="list-style-type: none"> ▪ Water Cycle Algorithm [21]. ▪ Modified Sine Cosine technique [23] ▪ Lightning Attachment Procedure Optimization [25] ▪ Improved Gravitational Search technique [27] ▪ Gravitational Search Algorithm [28] ▪ Slime Mould Algorithm [29] 	<ul style="list-style-type: none"> ▪ Biogeography-Based Optimization [22] ▪ Harmony Search technique [24] ▪ Teaching Learning-Based technique [26]
Hybrid-Based Algorithms	
<ul style="list-style-type: none"> ▪ The PSO and the tabu-search technique [30] ▪ The Salp Swarm technique with Simulated Annealing [15] ▪ Hybrid PSO and the Grey Wolf Optimization [31] ▪ Hybrid PSO and Gravitational Search Algorithm [32] 	

Few optimizers solved SORPD considering the uncertainties of the power system, which was solved using different optimizers; in [33], the SORPD was solved using an improved marine predator algorithm, and the uncertainties were presented using the scenario-based method. An improved version of the lightning attachment procedure optimization was presented for the ORPD solution with RERs and load uncertainties, also based on the scenario-based method [34]. However, while the scenario-based method is simple to apply, the obtained solution is an approximate solution. An enhanced grey wolf optimizer was implemented for the SORPD and considered the load uncertainty only [10]. In [11], the SORPD was solved by the Moth Swarm Algorithm, considering the RERs and loading uncertainties. S.M. Mohseni-Bonab et al. solved the SORPD for power loss and voltage deviation reduction with the application of the two-point estimate method for modeling the uncertainties in a system [35]. In [32], the Particle Swarm Optimization Gravitational Search Algorithm (FPSOGSA) was proposed for solving the SORPD with

uncertainties of the load demand, the PV's power and the WT's power. The quantum-behaved particle swarm optimization differential mutation (QPSODM) was implemented to solve the SORPD in the IEEE 14-bus and practical Adrar's isolated power system [36].

The MRFO is an efficient optimization method that has been employed to optimize a set of problems. However, there are some shortcomings related to the MRFO, including its premature convergence and its stagnation in cases of solving high nonlinear, complex and non-convex problems [37]. Thus, several modifications were implemented to boost the exploitation and exploration mechanisms of the MRFO. In a hybrid version of MRFO, a Gradient-Based Optimizer was proposed to solve the economic dispatch [38]. An improved MRFO was proposed based on Opposition-based learning (OBL) to solve the image segmentation problem of COVID-19 CT images [39]. An enhanced MRFO based on a chaotic mutation has been presented to solve the energy management of an MG [40]. In [41], a modified MRFO was presented based on an elite search pool (ESP) to enhance the searching skills of conventional MRFO.

MRFO was selected to solve the ORPD due to its unique and robust searching ability, which depended upon the chain foraging, cyclone foraging and somersault foraging of searching mechanisms. However, the MRFO suffers from the stagnation of highly nonlinear optimization problems such as ORPD and the SORPD. Thus, the AMRFO is a developed version of the MRFO that enhances its searching abilities and boosts its exploitation and exploration phases, which can be improved concurrently using three efficient improvement methods strategies including the fitness distance balance selection (FDB), Quasi Oppositional based learning (QOBL), and an adaptive Levy Flight (ALF). The contributions of this work are outlined as follows:

1. We propose a developed Adaptive Manta-Ray Foraging Optimization algorithm (AMRFO) for optimizing ORPD and SORPD.
2. We solve the SORPD under the uncertainties of the loading and the output power of the WTs.
3. We assess the performance of the system with and without the inclusion of the WTs for the total expected power loss and the total expected VDs.
4. An extensive comparison is presented between the proposed algorithm with different algorithms, including SCSO, WOA, DO, AHA, and the conventional MRFO, to verify the effectiveness of the AMRFO on a standard benchmark function and IEEE 30-bus system.

The following sections are provided: Section 2 introduces the problem formulation of the ORPD and the SORPD involving the objective functions and the constraints of the system. Section 3 explains the methodology of the uncertainties modeling of the system. Section 4 presents an overview of the MRFO and the suggested AMRFO. Section 5 lists the yielded results on an IEEE 30-bus system under the ORPD solutions. Section 6 provides the paper's conclusions.

2. Problem Formulation

The aim of the ORPD is to assign the best setting of the system's components involving the voltages, the transformer taps and the output Vars of the capacitors with constraints satisfaction. Generally, the ORPD problem can be provided as follows:

$$\text{Min } F(u, x) \quad (1)$$

In which

$$g_k(u, x) = 0 \quad (2)$$

$$h_n(u, x) \leq 0 \quad (3)$$

where F represents the objective function. u and x refer to the dependent and the control variables, respectively, which can be described as follows:

$$u = [V_G, Q_C, T_p] \quad (4)$$

$$x = [P_1, V_L, Q_G, S_T] \tag{5}$$

where T_p , Q_C and V_G are the tap ratio of the transformers, the injected Vars of the capacitors and the voltages of the generators, respectively. P_1 , S_T , Q_G , and V_L are the slack bus's power, the power flow in the transmission lines, the generators' reactive powers and the voltages at the load buses, respectively. The studied fitness functions are represented in the following subsections:

2.1. Objective Functions

2.1.1. The Power Loss (P_{Loss})

$$P_{Loss} = \sum_{i=1}^{NTL} G_{mn} (V_m^2 + V_n^2 - 2V_m V_n \cos \delta_{mn}) \tag{6}$$

where NTL is the No. of transmission lines (TLs). V_m and V_n are the voltage magnitudes at buses m and n , respectively. G_{mn} refers to TL's conductance between buses m and n .

2.1.2. The Voltage Deviations (VD)

$$VD = \sum_{i=1}^{NBL} |(V_i - 1)| \tag{7}$$

where NBL is the No. of load buses.

2.1.3. The Total Expected Power Losses (TEPL)

$$TEPL = \sum_{k=1}^{N_S} EPL_k = \sum_{k=1}^{N_S} \sigma_k \times P_{Loss,k} \tag{8}$$

where N_S represents the number generated scenario. σ_k and EPL_k are the probability and the expected power loss of the k -th scenario.

2.1.4. The Total Expected Voltage Deviations (TEVD)

$$TEVD = \sum_{k=1}^{N_S} EVD_k = \sum_{k=1}^{N_S} \sigma_k \times VD_k \tag{9}$$

EVD_i refers to the expected VD of the k -th scenario.

2.2. The System Constraints

The operating constraints involve equality and inequality bonds. The inequality constraints represent the allowable boundaries of the system components, while equality constraints refer to the balance of the power flow in the electric system [42]:

2.2.1. Equality Constraints

$$\sum_{i=1}^{NG} P_{Gi} - \sum_{i=1}^{NBL} P_{Li} = |V_i| \sum_{j=1}^{NTL} |V_j| (G_{ij} \cos \delta_{ij} + B_{ij} \sin \delta_{ij}) \tag{10}$$

$$\sum_{i=1}^{NG} Q_{Gi} - \sum_{i=1}^{NBL} Q_{Li} = |V_i| \sum_{j=1}^{NTL} |V_j| (G_{ij} \sin \delta_{ij} - B_{ij} \cos \delta_{ij}) \tag{11}$$

where P_G is the generated active power and Q_G is the reactive power. P_L and Q_L refer to the real and the reactive load powers. NG, NTL and NBL are No. generators, TLs and load buses, respectively.

2.2.2. Inequality Constraints

$$P_{G,k}^{min} \leq P_{Gk} \leq P_{G,k}^{max} \forall k \in NG \tag{12}$$

$$Q_{G,k}^{min} \leq Q_{G,k} \leq Q_{G,k}^{max} \forall k \in NG \tag{13}$$

$$V_{G,k}^{min} \leq V_{G,k} \leq V_{G,k}^{max} \forall k \in NG \tag{14}$$

$$T_n^{min} \leq T_n \leq T_n^{max} \forall n \in NT \tag{15}$$

$$Q_{C,n}^{min} \leq Q_{C,n} \leq Q_{C,n}^{max} \forall n \in NC \tag{16}$$

$$S_{T,n} \leq S_{T,n}^{min} \forall n \in NTL \tag{17}$$

$$V_k^{min} \leq V_k \leq V_k^{max} \forall k \in NBL \tag{18}$$

where *NC* and *NT* are the No. of the capacitors and transformers, respectively. The max and min superscript terms refer to the higher and lower boundaries of the variables. To ensure that the yielded solution is a proper solution, these constraints should be considered with the objective function using the weighted penalty sum method; this can be described as follows:

$$\begin{aligned}
 F = F_i + \varphi_1 (P_{G1} - P_{G1}^{lim})^2 + \varphi_2 \sum_{i=1}^{N_G} (Q_{Gi} - Q_{Gi}^{lim})^2 \\
 + \varphi_3 \sum_{i=1}^{N_Q} (V_{Li} - V_{Li}^{lim})^2 \\
 + \varphi_4 \sum_{i=1}^{N_I} (S_{Li} - S_{Li}^{lim})^2
 \end{aligned} \tag{19}$$

where $\varphi_1, \varphi_2, \varphi_3$ and φ_4 are penalty factors. *lim* is a superscript that refers to the upper or lower boundaries of the variables.

3. The Uncertainty Representation

The SORPD was solved with two uncertain parameters involving the speed of the wind and the loading. The loading uncertainty was modeled using the normal PDF based on its mean (μ_d) and the standard deviation (σ_d) as follows [43]:

$$f_d(P_d) = \frac{1}{\sigma_d \sqrt{2\pi}} \exp \left[-\frac{(P_d - \mu_d)^2}{2\sigma_d^2} \right] \tag{20}$$

The speed wind uncertainty was represented by the Weibull PDF based on its scale (λ) and shape (k) parameters using (21) [44].

$$f_v(v) = \frac{k}{\lambda} \left(\frac{v}{\lambda}\right)^{k-1} \exp \left[-\left(\frac{v}{\lambda}\right)^k \right] \tag{21}$$

The generated power from the WT (P_w) could be calculated from (22) [45].

$$P_w(v) = \begin{cases} 0 & \text{for } v < v_{in} \ \& \ v_{\omega} > v_{\omega o} \\ P_r \left(\frac{v-v_{in}}{v_r-v_{in}} \right) & \text{for } (v_{in} \leq v \leq v_r) \\ P_{wr} & \text{for } (v_{\omega r} < v \leq v_o) \end{cases} \tag{22}$$

where P_r is the WT's rated power. v_{in} , v_r and v_o refer to the cut-in, rated and cut-out speeds of WT, respectively.

Here, The MCS was employed to generate a set of scenarios based on the PDFs of the load demand and the wind speed [46]. In this paper, the mean (μ_d) is 70, and the standard deviation (σ_d) is 10 [47]. The Weibull PDF, based on its scale (λ) and shape (k) parameters,

was selected to be nine and two, respectively [48]. In this paper, 1000 MCSs were conducted, and a set of samples for the loading and speed of the wind were obtained, as depicted in Figures 1 and 2, respectively. The SBR method is a common method that was implemented to reduce the huge number of scenarios that had been generated from the MCS method. The steps of the SBR method are depicted as follows in [49,50]:

Step 1: A vector is constructed that includes the uncertain parameters of the load demand and the wind speed as follows:

$$H_k = [S_{L,k}, v_{s,k}] \quad \forall i \in N_0 \tag{23}$$

where N_0 refers to MCS's number for the generated scenarios.

Step 2: The probability values of the generated scenarios is $\sigma_k = 1/N_0$. The norm distance between each pair of scenarios is calculated using (27) as follows:

$$D_{i,j} = \|H_i - H_j\| \tag{24}$$

Step 3: The D matrix is constructed, which is a square matrix, and its dimension is $N_0 \times N_0$. The required number of reduced scenarios is selected.

Step 4: The lowest distance value and the corresponding probability for the (i, j) scenario are assigned. It is then assumed that the two rows correspond to scenarios m (row m) and n (row n), respectively, with probabilities of σ_m and σ_n .

Step 5: If $\sigma_m \geq \sigma_n$, scenario n is removed. Then probability is updated $\sigma_m = \sigma_m + \sigma_n$. Otherwise, scenario m is removed.

Step 6: If the stopping criteria are not satisfied, the previous steps are repeated.

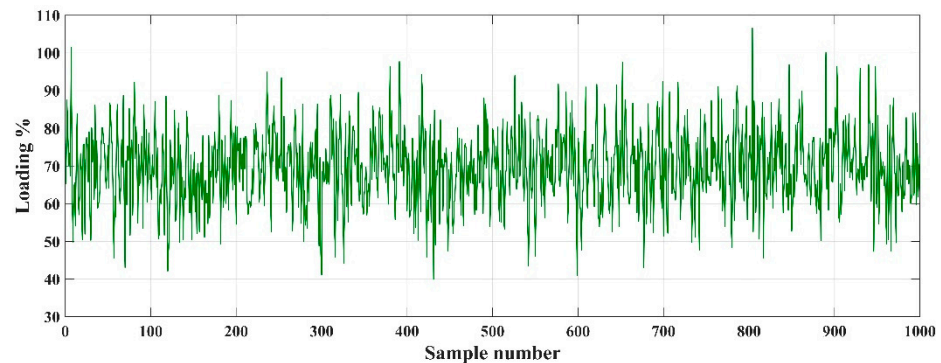


Figure 1. The generated scenario of the load demand by MCS.

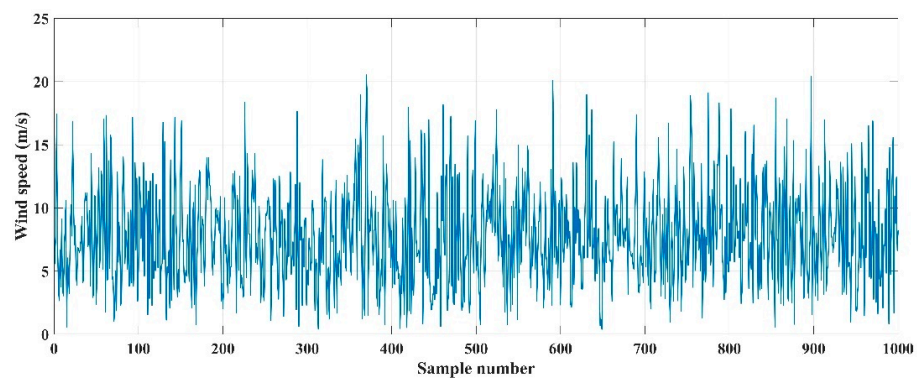


Figure 2. The wind speed scenarios by MCS.

The scenario-based reduction (SBR) method was implemented to reduce a large number of the generated scenario and diminish the computational burden. Ten scenarios generated the application of SBR, the probabilities of each scenario, and the associated wind speed and loading, which are provided in Table 2.

Table 2. The generated scenarios by uncertainties representation.

Scenario Number	Loading %	Wind Speed (m/s)	Probability (σ_i)
1	42.10	5.04	0.011
2	91.46	8.38	0.027
3	78.61	15.57	0.02
4	85.30	13.36	0.023
5	71.11	7.72	0.393
6	106.56	9.42	0.001
7	62.36	10.37	0.245
8	96.91	14.40	0.001
9	77.87	5.70	0.233
10	49.63	8.93	0.046

4. Optimization Algorithm

4.1. Manta Ray Foraging Optimization (MRFO)

The MRFO algorithm mimics the behavior of the manta rays' foraging behavior which is based on three movements, including cyclone foraging, chain foraging, and somersault foraging, to look for the abundant plankton area in oceans [37]. These three movements can be represented as follows:

4.1.1. Chain Foraging

In this phase, the manta rays move from a foraging chain when they move in one line. The manta rays proceed to the location that has an abundant concentration of plankton. This foraging stage is formulated using (25).

$$X_i^{t+1} = X_i^t + r(X_{best} - X_i^t) + \alpha(X_{best} - X_i^t) \tag{25}$$

Here, X_{best} refers to the best location planktons. r refers to a random solution between [0 and 1]. $\alpha = 2 \cdot r \cdot \sqrt{|\log(r)|}$

4.1.2. Cyclone Foraging

Here, the manta ray positions are updated in special motion around the best location of the plankton. The cyclone foraging is formulated according to the following equations:

$$X_i^{t+1} = \begin{cases} X_{best}(t) + r(X_{best}(t) - X_i^t) + \beta(X_{best} - X_i^t) & i = 1 \\ X_{best}(t) + r(X_{i-1}^t - X_i^t) + \beta(X_{best} - X_i^t) & i = 1, 2, \dots, n \end{cases} \tag{26}$$

in which:

$$\beta = 2e^{r_1 \frac{T-t+1}{T}} \cdot \sin(2\pi r_1) \tag{27}$$

where β represents a weight coefficient. t and T are the current and the maximum iteration numbers. r_1 and r represent the random values in [0, 1]. To improve the exploration process, the manta rays update their location randomly as follows:

$$X_i = Lb + rand \times (Ub - Lb) \tag{28}$$

$$X_i^{t+1} = \begin{cases} X_{rand} + r \times (X_{rand} - X_i^t) + \beta \times (X_{rand} - X_i^t) & i = 1 \\ X_{rand} + r \times (X_{i-1}^t - X_i^t) + \beta \times (X_{rand} - X_i^t) & i = 2, \dots, N \end{cases} \tag{29}$$

where X_{rand} represents the location of manta rays that are selected randomly from the populations.

4.1.3. Somersault Foraging

In this stage, the manta rays swim and move around in the food location, periodically somersaulting to move to a novel location. Subsequently, they continuously update their positions around the best place discovered thus far. This stage is formulated as:

$$X_i^{t+1} = X_i^t + S \cdot (r_2 \times X_{best} - r_3 \times X_i^t) \tag{30}$$

where r_2 and r_3 denote random numbers in the range of 0 to 1. S is a constant value that equals two.

4.2. The Adaptive Manta-Ray Foraging Optimization (AMRFO)

The AMRFO is based on three improvement techniques, including the fitness distance balance (FDS), adaptive Levy flight and the QOBL. The FDS method is a powerful selection method that can be utilized for the global searching ability improvement of algorithms [51].

4.2.1. The Fitness Distance Balance

The FDS is based on the distance between the candidate solutions and the best solution, as well as the fitness function values. Initially, this distance could be calculated, and the vector of the distance matrix constructed according to the following equations:

$$D_{X_i} = \sqrt{\left((x_{1[i]} - x_{1[best]})^2 + (x_{2[i]} - x_{2[best]})^2 + \dots + (x_{n[i]} - x_{n[best]})^2 \right)} \tag{31}$$

$$DX \equiv \begin{bmatrix} d_1 \\ \vdots \\ d_m \end{bmatrix}_{m \times 1} \tag{32}$$

The vector of the fitness function F was constructed as depicted in Equation (31).

$$F \equiv \begin{bmatrix} f_1 \\ \vdots \\ f_m \end{bmatrix}_{m \times 1} \tag{33}$$

The fitness values and the distance were normalized to determine the impact of the distance and fitness. In the FDS, the normalized distance and fitness values were used to find the score calculation of the candidates according to the following equation [51]:

$$S_{p_i} = w \times normF_i + (1 - w) \times normD_{X_i} \tag{34}$$

where w is a weight parameter in the range of 0 and 1 that characterizes the effect of the distance or fitness values.

4.2.2. The Quasi-Oppositional Based Learning (QOBL)

The second modification is the QOBL, which is an efficient method that can be applied for performance enhancement and searching abilities of several optimization algorithms [34]. The QOBL is a combination of the oppositional-based learning (OBL) mechanism along with the Quasi-based method that was applied with several optimization algorithms [52–55]. In the OLB, these populations update their placement to the opposite number or the mirror location of the population as follows:

$$X_{i,j}^o = Ub_j + Lb_j - X_{i,j}, \quad i = 1, 2, \dots, n \tag{35}$$

The oppositional-based method is the center point between the upper and the lower point as follows:

$$C_{i,j} = (Ub_j + Lb_j) / 2 \tag{36}$$

Finally, the QOBL could be described as follows:

For $i = 1:No. \text{ manta rays}$

For $j = 1:D$

$$X_{i,j}^o = Ub_j + Lb_j - X_{i,j}$$

$$C_{i,j} = (Ub_j + Lb_j) / 2$$

If $(X_{i,j} < C_{i,j})$

$$X_{i,j}^{qo} = C_{i,j} + (X_{i,j}^o - C_{i,j}) \times rand \tag{37}$$

else

$$X_{i,j}^{qo} = C_{i,j} + (C_{i,j} - X_{i,j}^o) \times rand \tag{38}$$

End

End

End

4.2.3. Adaptive Levy Flight (ALF)

The ALF has been used to boost the exploitation of the MRFO via updating the locations of the manta rays around the best location so far based on the adaptive levy flight and according to the following equations:

$$X_i^{t+1} = r_3 X_{best} - r_4 X_i^t + C_1 \cdot L_F \cdot (X_r^t - X_i^t) \tag{39}$$

$$L_F = 0.05 \times \frac{u \times \sigma}{|v|^{1/\beta}} \tag{40}$$

$$\sigma = \left(\frac{\Gamma(1 + \beta) \times \sin(\pi\beta/2)}{\Gamma((1 + \beta)/2) \times \beta \times 2^{(\beta-1)/2}} \right)^{1/\beta} \tag{41}$$

X_r denotes the random location of the manta ray. $C_1 = 2r_4(1 - t/T)$. r_4 and r_5 refer to parameters in the range [0–1]. u and v refer to the random value obtained by the normal distribution. β was selected to be 1.5. The procedure for solving SORPD with the proposed technique is illustrated in Figure 3.

The computational complexity of the AMRFO is based on chain foraging, cyclone foraging, the somersault foraging phases, FDB, QOBL and levy flight motion which can be described as follows:

$$O(MRFO) = O(T(O(\text{cyclone foraging} + \text{chain foraging}) + O(\text{somersault foraging}) + O(\text{FDB}) + O(\text{QOBL}) + O(\text{Levy flight motion}))) \tag{42}$$

$$O(MRFO) = O(T(nd + nd + nd + nd + nd)) = O(T(5 \times nd)) \tag{43}$$

where n , d and T denote the numbers of the populations, the variables and the maximum number of iterations.

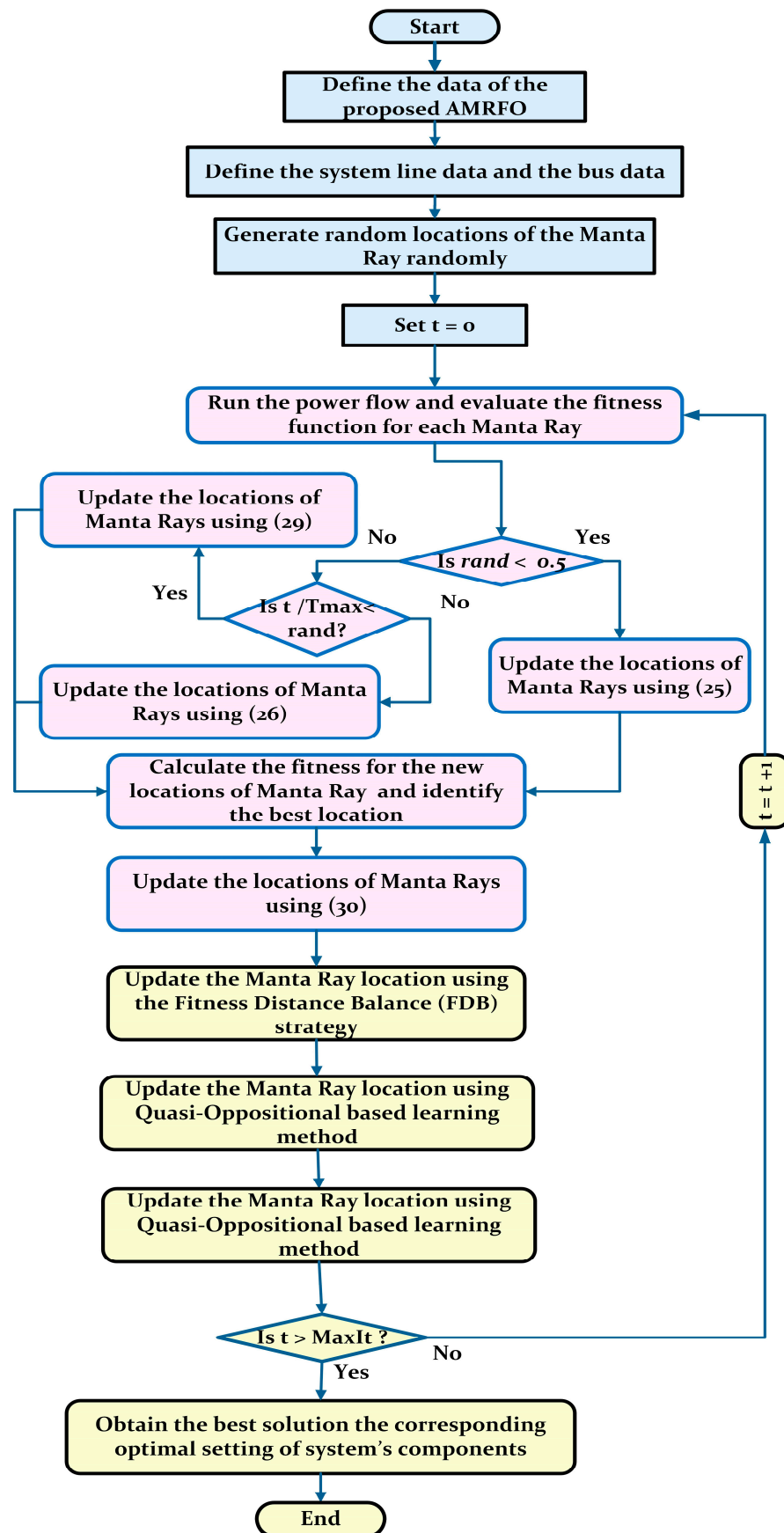


Figure 3. Flow chart of AMRFO application for the ORPD.

5. Results and Discussion

5.1. Application of the AMRFO on Standard Benchmark Functions

Here, the proposed AMRFO was applied and tested on 23 standard benchmark functions. The program was conducted on a PC with Core I7 @ 2.90 GHz and 32 GB RAM by MATLAB software (R2021a). The acquired results by the AMRFO were compared with other optimization approaches, including the Sand Cat Swarm Optimization (SCSO) [56], Grey Wolf Optimizer (GWO) [57], the Whale Optimization Algorithm (WOA) [58], Artificial Hummingbird Algorithm (AHA) [59], Dandelion Optimizer (DO) [60], and the standard MRFO [37]. Table 3 provides the parameters of the optimizers. It should be highlighted here that for a fair comparison, the number of the populations and the maximum number of iterations were selected to be the same, while the other parameters of the SCSO, GWO, WOA, AHA and DO, were selected similarly to [56–60]. Three types of these standard functions were considered where F1 to F7 were Unimodal functions, F8 to F13 were Multimodal functions, and F14 to F23 were Fixed-dimension multimodal functions [61–63]. It should be highlighted here that the dimensions of the first 13 objective functions were 30, while the dimensions of F14, F16, F17 and F18 were 2. Furthermore, the dimensions of F15, F21, F22 and F23 were four, and the dimensions of F19 were three, and F20 were six.

Table 3. The parameters of the studied optimizers.

Algorithm	The Parameters
SCSO [56]	Max. iterations = 250, No. populations = 25, Phases control range (R) in range $[-2rg, 2rg]$, Sensitivity range (rg) = $[2, 0]$.
GWO [57]	Max. iterations = 250, No. populations = 25, $a = [2, 0]$, $A = [2, 0]$, $C = 2 \cdot \text{rand}(0, 1)$
WOA [58]	Max. iterations = 250, No. populations = 25, $a = [2, 0]$, $A = [2, 0]$, $l = [1, -1]$, $b = 1$.
AHA [59]	Max. iterations = 250, NO. populations = 25
DO [60]	Max. iterations = 250, No. populations = 25, $\alpha = [0, 1]$, $k = [0, 1]$.
MRFO [37]	Max. iterations = 100, No. populations = 25, $S = 2$.
AMRFO	Max. iterations = 100, No. populations = 25, $S = 2$.

The numerical results for the standard benchmark functions with the application of the studied optimization methods are listed in Appendix A in Table A1. The best, the worst and mean values, p -value, and the standard deviation (sd) of 25 trail runs are depicted in Table A1. Referring to Table A1, the proposed AMRFO could provide very competitive results for the unimodal functions (F1 to F7), multimodal functions (F8 to F13), and the fixed dimension (F14 to F23). It is worth mentioning here that the results for F9 of the SCSO, AHA, MRFO, and the proposed AMRFO were converged rapidly as well as for F10, F11, F13, F17, F18, F19 and F20. Figure 4 shows the convergence curves which were obtained by the studied optimizers. According to Figure 4, the objective functions converged rapidly by the suggested AMRFO compared to the other well-known optimizers. However, in some cases, other optimizers converged to the best solution better than AMRFO, such as AHA, SCSO, WOA, and MRFO for F9. Likewise, for F11 and F13. The Wilcoxon test was carried out, and the P-Value between the proposed AMRFO and the other techniques is provided in the 7th column of Table A1. If the p -value was greater than 5%, it suggested that there was no statistically significant difference between these two optimizers. Conversely, if the p -value was less than 5%, it indicated that there was a statistically significant difference between these algorithms. Furthermore, if the value of the p -value was N/A. “-” and was referred to as “not applicable”, which meant that the corresponding optimizer could not statistically compare with itself in the rank-sum test, while “N/A” referred to “not available”; this meant that the difference in the results was identical and could not be statistically compared in terms of the rank-sum test. The ranking of the Friedman test is listed in the last column of Table A1, and the average ranking is depicted in Figure 5. It is clear that the proposed AMRFO was ranked best among the tested algorithms. According to the reported values,

there were significant differences between the suggested AMRFO and SCSO, WOA, GWO, AHA, DO, and the conventional MRFO for most cases. However, there were no significant differences between AMRFO and WOA for F8, F9 and F11. The boxplots of AMRFO and SCSO, WOA, GWO, AHA, DO, and the conventional MRFO for the benchmark functions are provided in Figure 6. From the depicted boxplots, the suggested AMRFO had narrow boxplots, which verified that the distribution of the obtained results went well for this optimizer compared to the other techniques for most functions except for F20, where AHA and DO were the best.

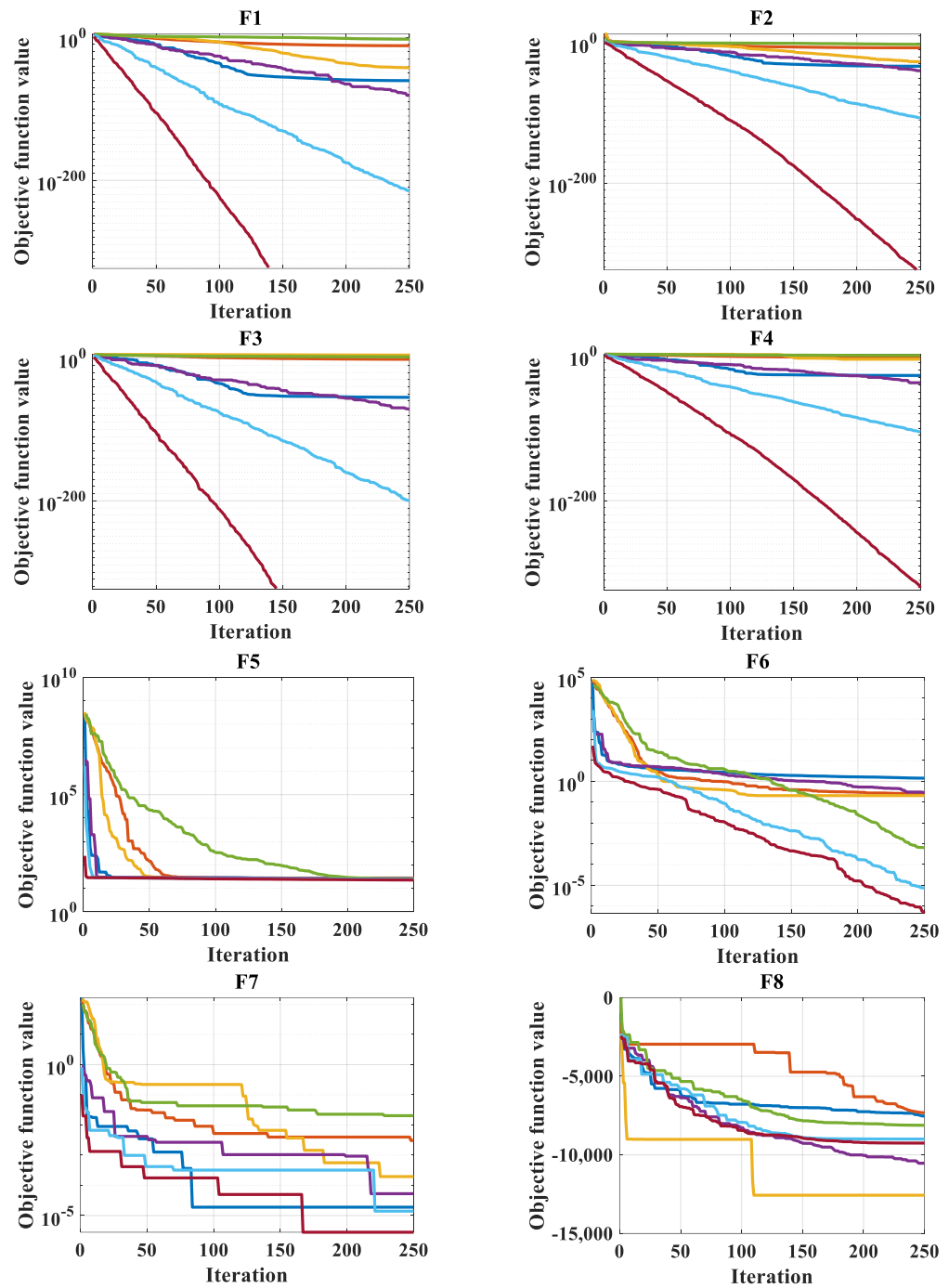


Figure 4. Cont.

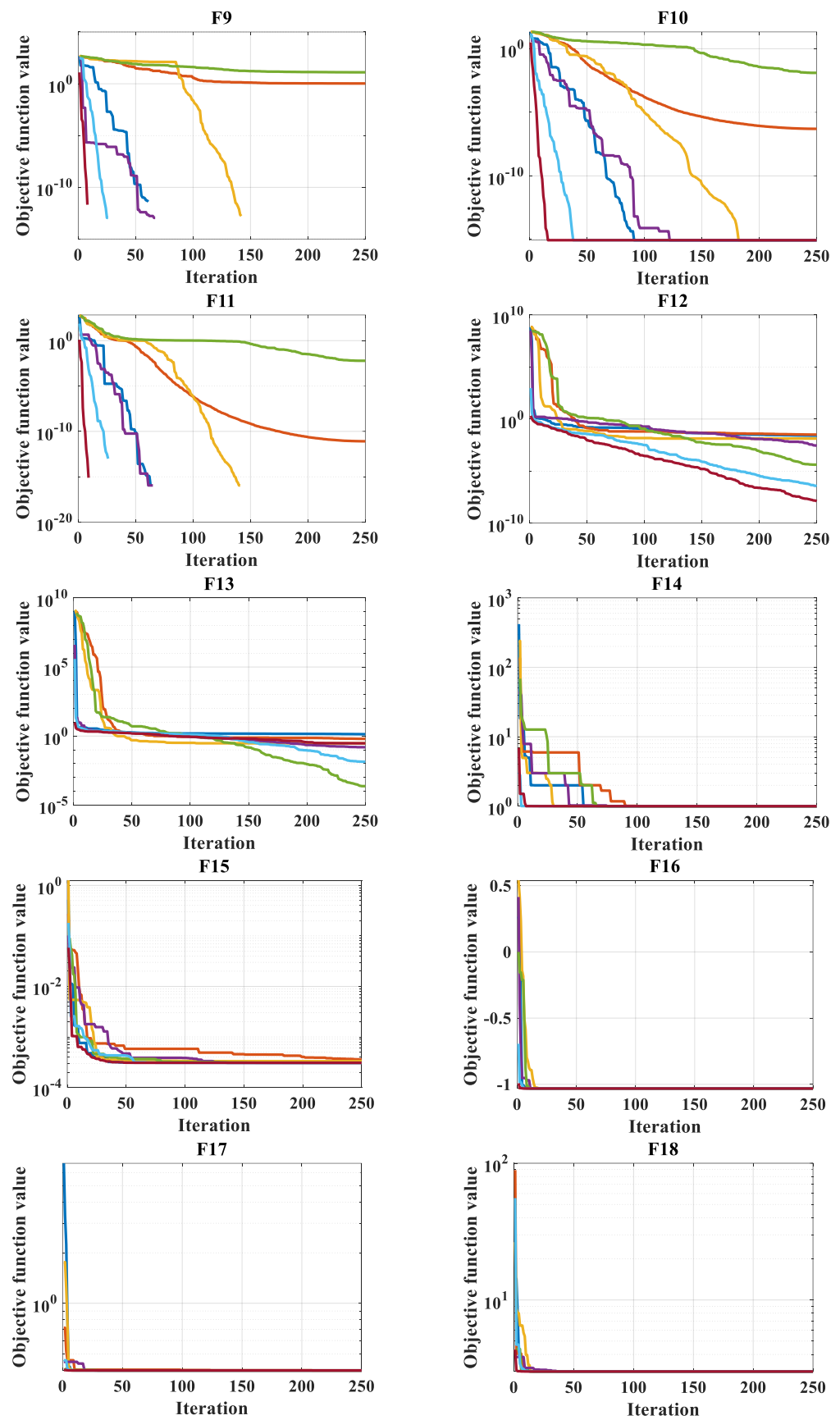


Figure 4. Cont.

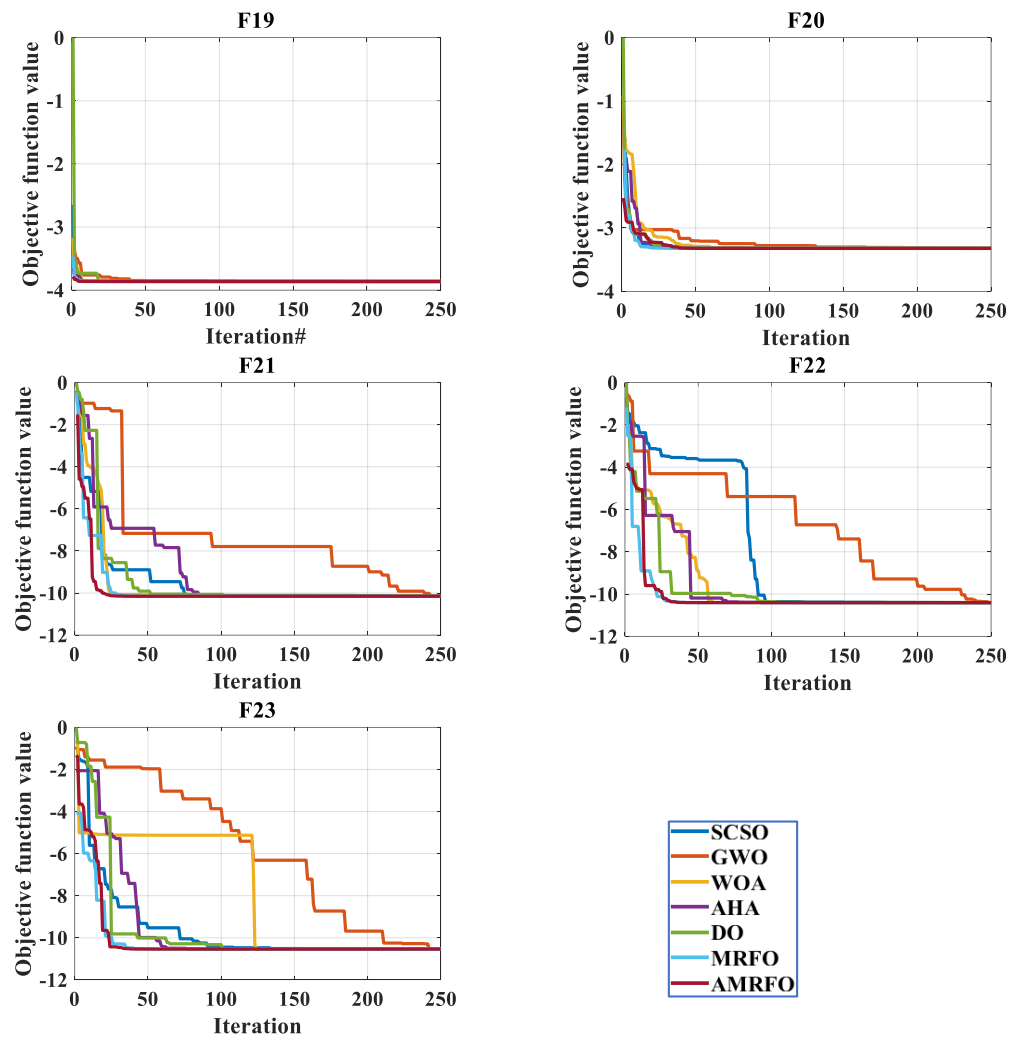


Figure 4. Convergence curves of the studied benchmark functions.

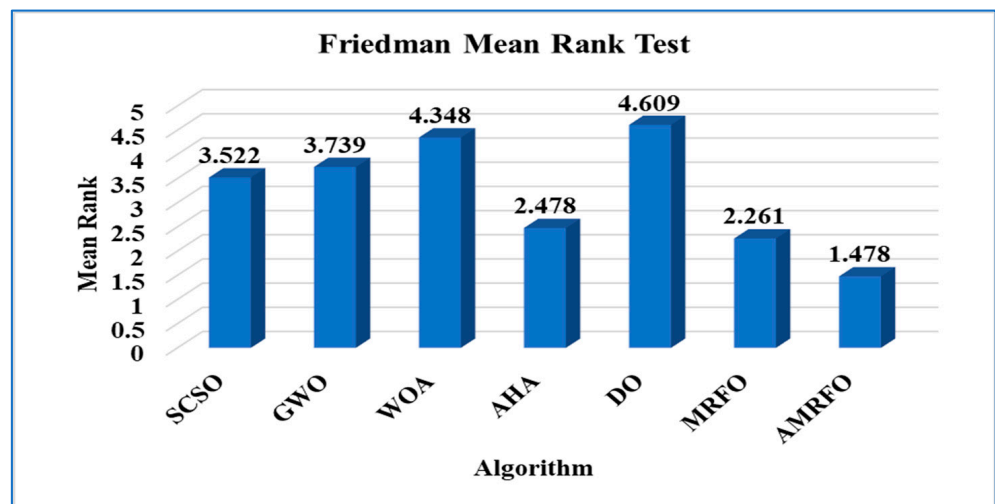


Figure 5. The average ranking results of the Friedman test.

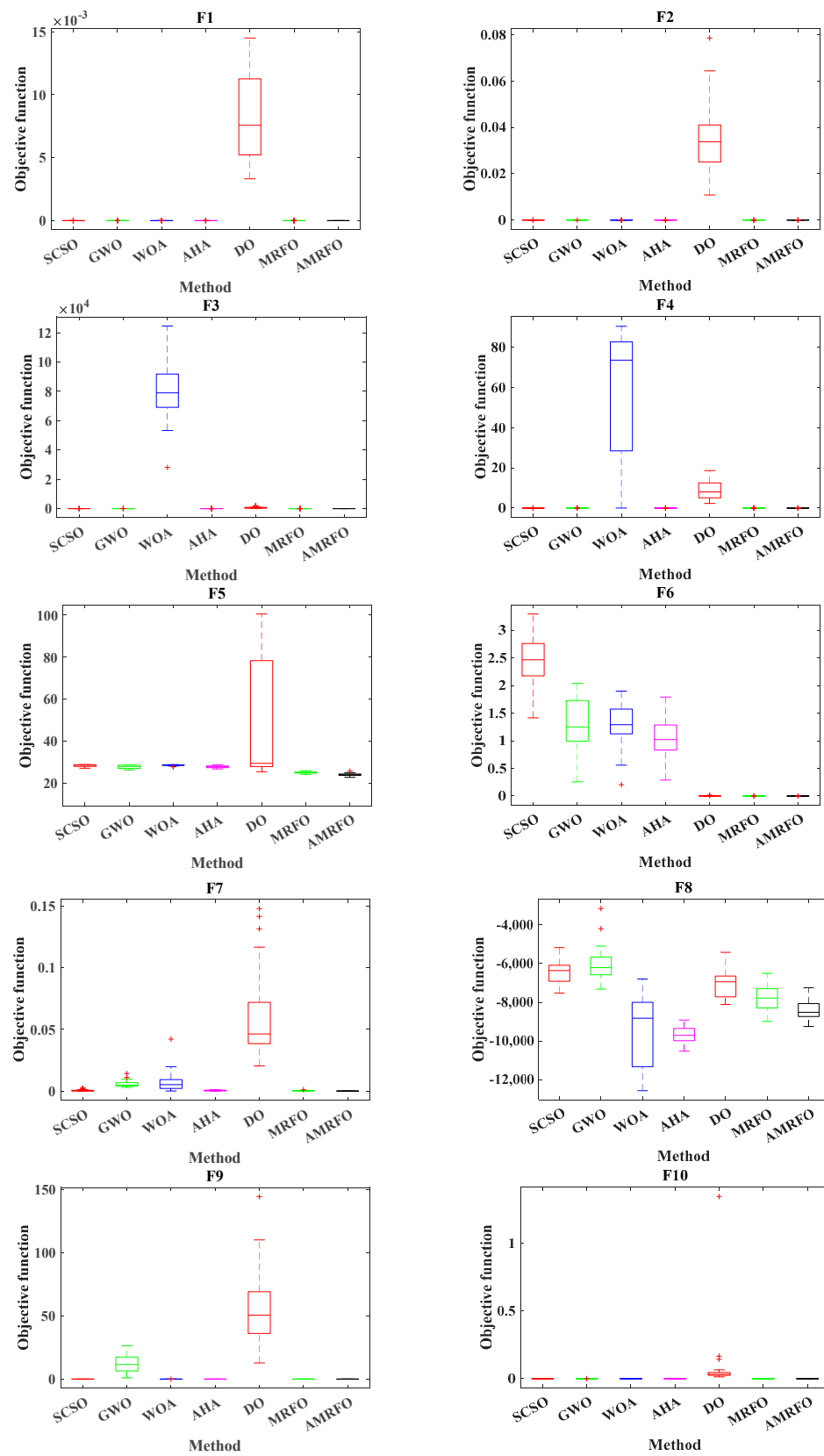


Figure 6. Cont.

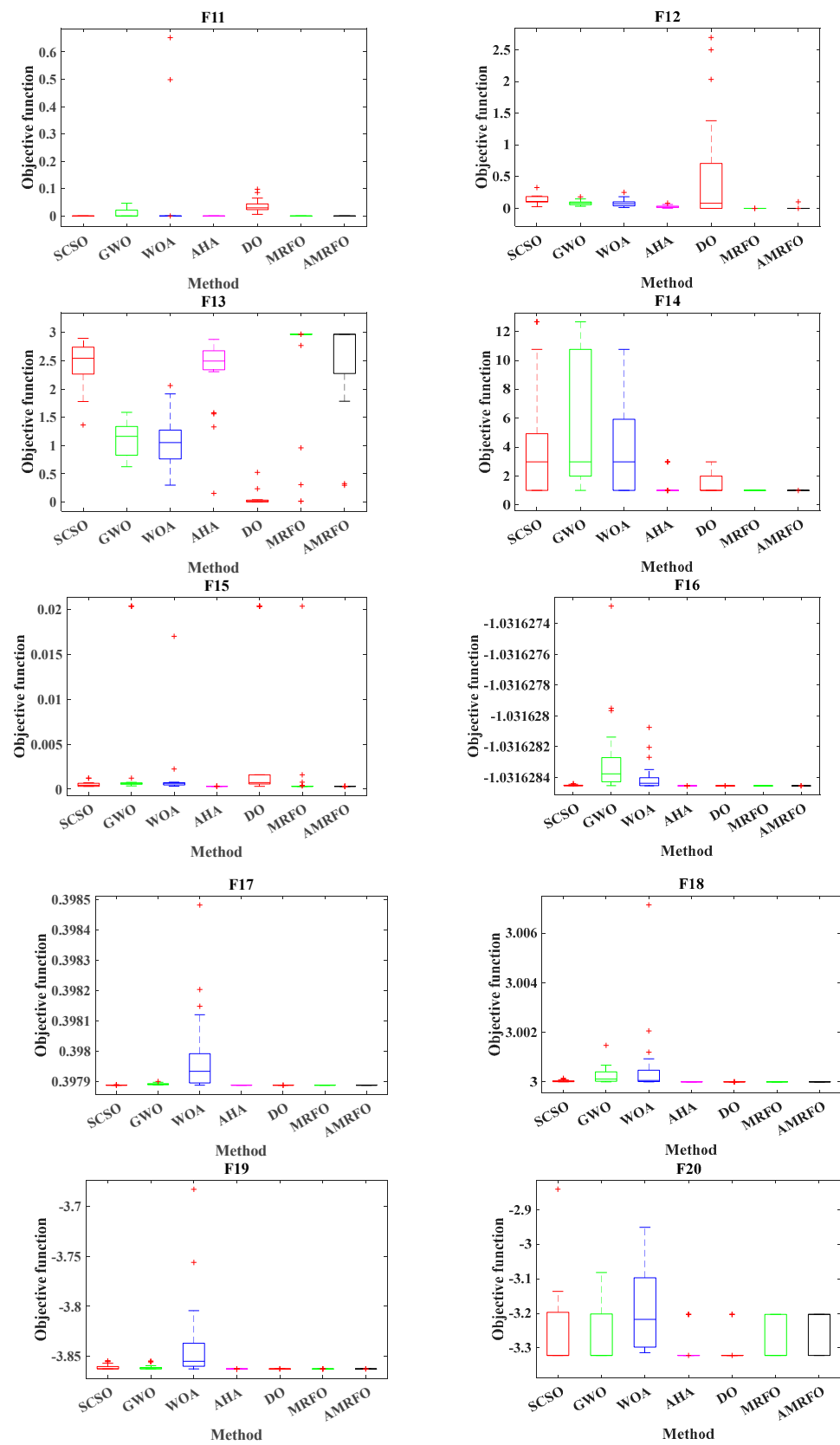


Figure 6. Cont.

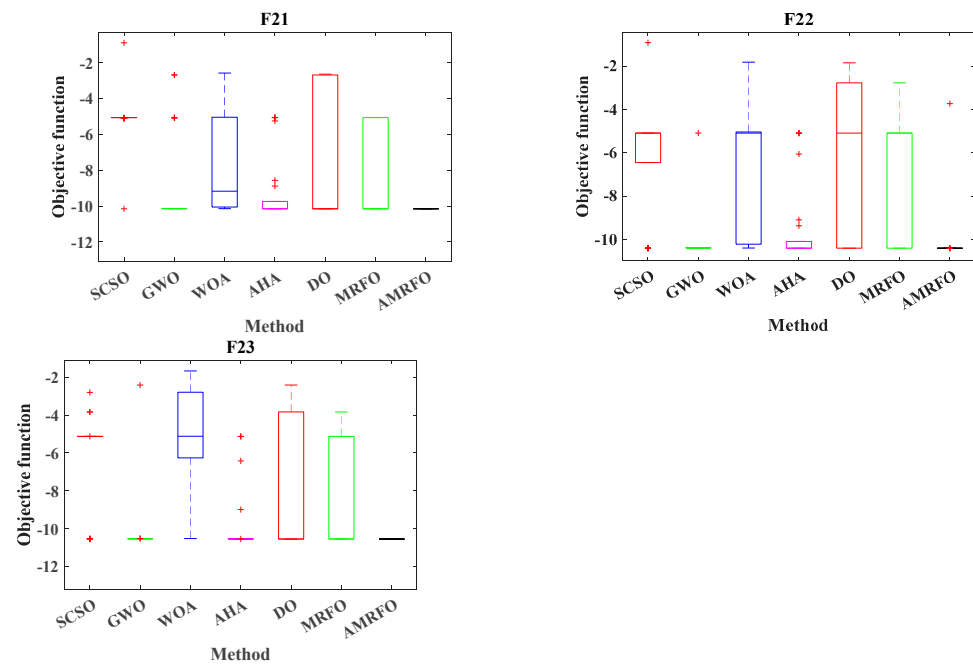


Figure 6. Boxplot for the studied benchmark functions.

5.2. Application the AMRFO for Solving the ORPD Problems

The suggested AMRFO was used to optimize the conventional ORPD and the SORPD for the IEEE 30-bus system. The system load was 283.4 MW + j126.2 MVAR [64] and consisted of 4 transformers, 6 generators, 9 capacitor bank units and 41 transmission lines. The voltage limits of the load buses were between [0.95–1.05]. The voltage limits at the generation units were [0.95–1.1]. The injected reactive power by capacitors was in the range of [0–5], while the boundaries of the transformer tap setting were [0.9–1.1] [65]. The parameters of the studied algorithms were selected the same as in Table 3, except that the Max. iterations and No. of populations were 100 and 20 for the conventional ORPD while, for SORPD, these values were 150 and 50, respectively. The studied cases were outlined as follows:

5.2.1. Case 1: Solving the Conventional OPRD

The suggested AMRFO solved the ORPD for two functions, including the power losses and VDs’ reduction. Initially, the value of the power loss was 5.596 MW, while the VDs were 0.8691 p.u., respectively. In the case of its application, the proposed AMRFO for loss reduction and the power loss was reduced to 4.5279 MW or by 19.09% compared to the initial case. The optimal setting of the control variables that were obtained is listed in the 4th column of Table 4. An extensive comparison of the loss reduction with other optimizers is provided in Table 5. As provided in Table 5, the best-yielded results were captured by the proposed algorithm. In other words, the power loss reductions compared to the based case were obtained by the suggested AMRFO, MRFO, SCSO, GWO, WOA, AHA, DO, MPA, JA [66], ALO [18], HSA [24], PSO [24], STGA [24], TLBO [26], QOTLBO [26], DE [8], SGA [12], FA [67], HPSO-TS [30], TS [30], PSO [30], WOA [17], PSO-TVAC [17], IDE [16], BBO [22], CLPSO [19], PSO [19], GSA [27], PSO [27], GSA-CSS [27], and IGSA-CSS [27], which were 19.09%, 19.04%, 18.01%, 17.27%, 16.35%, 11.95%, 18.65%, 18.99%, 17.35%, 17.98%, 12.33%, 12.01%, 11.71%, 18.46%, 18.52%, 18.6%, 18.35%, 18.35%, 19.2%, 12.07%, 16.26%, 17.9%, 16.96%, 18.65%, 18.67%, 17.29%, 18.49%, 10.48%, 12.16%, 14.35%, and 14.83%, respectively. The trends of the power losses of the AMRFO, MRFO, SCSO, GWO, WOA, AHA, and DO algorithms are shown in Figure 7. The proposed AMRFO has stable convergence characteristics and converges at the 81st iteration, as shown in Figure 7.

Table 4. The simulation results and optimal control variables from the conventional ORPD.

Control Variables	Min.	Max.	P_{Loss} Minimization	VD Minimization
V1	0.9	1.1	1.100	1.006
V2	0.9	1.1	1.094	1.007
V5	0.9	1.1	1.073	1.069
V8	0.9	1.1	1.075	1.000
V11	0.9	1.1	1.098	1.031
V13	0.9	1.1	1.100	1.024
T11	0.9	1.1	1.000	1.040
T12	0.9	1.1	0.930	0.910
T15	0.9	1.1	0.980	1.000
T36	0.9	1.1	0.970	0.970
Q10	0	0.05	2.500	4.570
Q12	0	0.05	4.840	0.380
Q15	0	0.05	4.770	4.810
Q17	0	0.05	4.760	0.870
Q20	0	0.05	4.140	4.740
Q21	0	0.05	4.930	4.980
Q23	0	0.05	3.950	4.970
Q24	0	0.05	4.920	4.850
Q29	0	0.05	2.430	2.850
P_{Loss} (MW)			4.5279	5.7852
VD(p.u)			1.9829	0.0913
L_{max} (p.u)			0.1162	0.1367

Table 5. Statistical results for power loss reduction.

Algorithm	Worst	Mean	Best
AMRFO	4.6089	4.5488	4.5279
MRFO	4.6532	4.5740	4.5308
SCSO	4.7373	4.6537	4.5884
GWO	4.7321	4.6795	4.6295
WOA	4.9064	4.7969	4.6813
AHA	5.7434	5.1461	4.9275
DO	4.7657	4.6168	4.5526
Marine predator Algorithm(MPA) [68]	4.6006	4.55389	4.5335
Jaya Algorithm (JA) [66]	NA	NA	4.625
Ant Lion Optimizer (ALO) [18]	NA	NA	4.5900
Harmony Search Algorithm (HSO) [24]	4.9653	4.924	4.9059
PSO [24]	5.0576	4.972	4.9239
Standard Genetic Algorithm (SGA) [24]	5.1651	5.0378	4.9408
TLBO [26]	4.57480	4.56950	4.5629
Quasi-oppositional TLBO [26]	4.56170	4.56010	4.5594

Table 5. Cont.

Algorithm	Worst	Mean	Best
Differential Evolution (DE) [8]	NA	NA	4.5550
Specialized Genetic Algorithm (SpGA) [12]	NA	NA	4.5692
Firefly Algorithm (FA) [67]	4.59	4.578	4.5691
Hybrid PSO and Tabu search (HPSO-TS) [30]	NA	NA	4.5213
Tabu search (TS) [30]	NA	NA	4.9203
Whale Optimization Algorithm (WOA) [17]	NA	NA	4.5943
PSO [17]	NA	NA	4.6469
Improved Differential Evolution (IDE) [16]	NA	NA	4.5521
Biogeography-Based Optimization (BBO) [22]	NA	NA	4.5511
Comprehensive Learning PSO (CLPSO) [19]	NA	NA	4.6282
Gravitational Search Algorithm (GSA) [27]	NA	NA	5.00954
Improved GSA With Conditional Selection Strategies (IGSA-CSS) [27]	NA	NA	4.76601

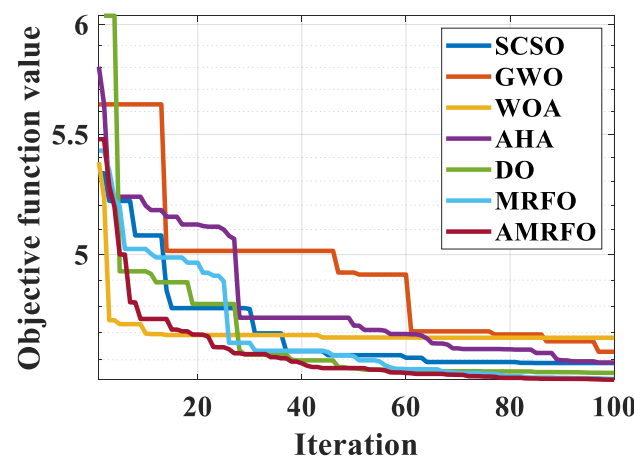


Figure 7. Convergence curves for loss reduction.

In the case of considering the second objective function (VDs reduction), VDs were reduced from 0.8691 p.u. to 0.0913 p.u. by the application of the proposed algorithm. The optimal control variables for VDs’ reduction are listed in the 5th column of Table 4. The extensive comparison between the suggested AMRFO and other algorithms for the VDs reduction is tabulated in Table 6, including the best, worst and mean values. Judging from Table 6, the minimum value of the VDs was obtained by the application of the suggested AMRFO. This was in addition to the percentage reductions of the VDs which were obtained by the proposed AMRFO, MRFO, SCSO, GWO, WOA, AHA, DO, PSO-TVIW [69], SPSO-TVAC [69], PSO-TVA [69], PSO-CF [69], PG-PSO [69], SWT-PSO [69], SSO [15], HSSSA [15], MSSA [15], SSA [15], CSA [15], ALO [13], GSA [18,27], PSO [27], which were GSA-CSS [27] are 89.49%, 88.01%, 84.60%, 84.40%, 79.88%, 76.11%, 85.41%, 88.06%, 84.42%, 76.25%, 85.19%, 86.17%, 81.43%, 77.79%, 79.90%, 73.53%, 78.32%, 85.40%, 86.28%, 80.16%, 87.96%, and 85.74%, respectively. The trends of the VDs with iterative progress using different algorithms are provided in Figure 8. Referring to this figure, the suggested AMRFO had stable convergence characteristics where it converged at the 88th iteration. The boxplot is a standard method that has been used to show the distribution of the obtained results. Figures 9 and 10 show the boxplots of different optimization algorithms for the power loss and VDs, respectively. From Figures 9 and 10, the proposed AMRFO had narrow boxplots for the two cases, which verified the efficiency of the AMRFO.

Table 6. Statistical results for VDs’ minimization.

Algorithm	Worst	Mean	Best
AMRFO	0.1218	0.1068	0.0913
MRFO	0.1309	0.1158	0.1042
SCSO	0.2174	0.1722	0.1338
GWO	0.2021	0.1707	0.1356
WOA	0.5001	0.2556	0.1749
AHA	0.6492	0.3860	0.2076
DO	0.1939	0.1460	0.1268
PSO based TVAC [69]	0.5791	0.1597	0.1038
PSO with TVAC [69]	0.5796	0.2376	0.2064
PG-PSO [69]	0.2593	0.1440	0.1202
Social Spider Optimization [15]	0.42681	0.2863	0.19304
Hybrid Salp Swarm Algorithm with Simulated Annealing [15]	0.576439	0.308337	0.174701
Modified Salp Swarm Algorithm (MSSA) [15]	1.860037	0.690254	0.230087
Salp Swarm Algorithm (SSA) [15]	0.941759	0.374529	0.188411
Cuckoo search algorithm (CSA) [15]	0.2076	0.16432	0.12692
Ant Lion Optimizer (ALO) [13]	NA	0.1575	0.1192
Gravitational Search (GS) [27]	NA	NA	0.17241
GSA and Conditional Selection Strategies (GSA-CSS)	NA	NA	0.12394

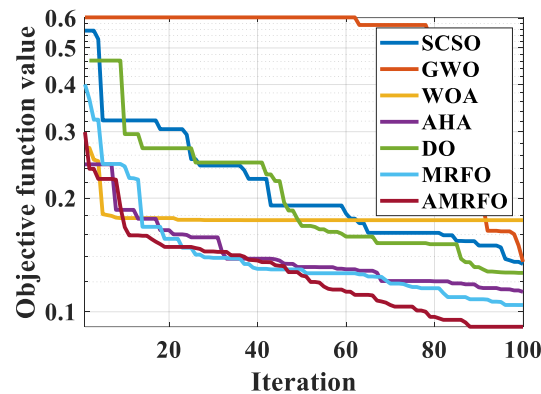


Figure 8. The convergence curves for VDs’ reduction.

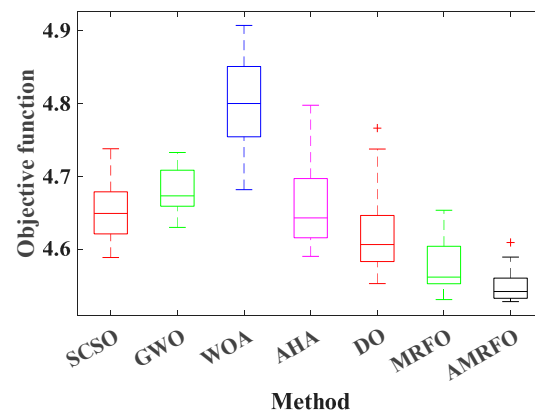


Figure 9. The boxplots of the power losses caused by the studied optimizers.

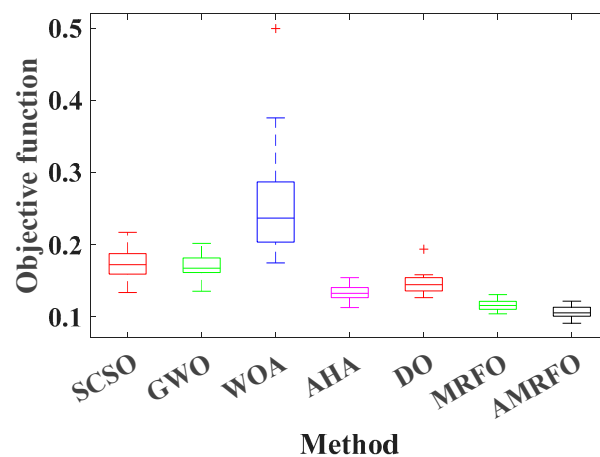


Figure 10. Boxplots of the VDs through the studied optimizers.

5.2.2. Case 2: Solving the SORPD

In this section, the suggested AMRFO solved the SORPD when considering the uncertainties of the loading and WTs’ output powers. In this paper, the wind farm contained 25×3 MW turbines, and the cut-in, rated, and cut-out speeds of the wind turbines were 3, 16, and 25 m/s, respectively [30]. The two objective functions have been considered with the SORPD solution, including the total expected power loss (TEPL) and the total expected voltage deviations (TEVD). In the base case (without solving the SORPD and without WTs), the TEPL and the TEVD were 5.1025 MW and 0.7919 p.u. The system voltage profile at the base case is shown in Figure 10. In the case of solving the SORPD without the inclusion of WTs, TEPL decreased from 5.1025 MW to 4.5201 MW. The results of this case are depicted in Table 7, including the percentage load at each scenario, the values of P_{Loss} , the expected power loss (EPL), the VD and the expected VDs (EVD). Referring to Table 7, the highest power loss values were in scenarios number 2, 6, and 8 because the values of the loading were high in these scenarios. Furthermore, the highest value of the EPL was scenario number 5 because the probability of this scenario was the highest. In the case of solving SORPD with the inclusion of the WTs, TEPL was reduced from 5.1025 MW to 2.9011 MW compared to the base case. In other words, TEPL was reduced from 4.5201 MW to 2.9011 MW with the inclusion of WTs. Table 8 tabulates the results for the TEPL with the inclusion of WTs.

Table 7. The simulation results of the SORPD solution for TEPL reduction without WTs.

Scenario No.	σ_i	Loading %	P_{Loss} (MW)	EPL(MW)	VD(p.u)	EVD(p.u)
1	0.011	42.10	2.3387	0.0257	0.3412	0.0038
2	0.027	91.46	9.1826	0.2479	0.5218	0.0141
3	0.02	78.61	5.9414	0.1188	0.5981	0.0120
4	0.023	85.30	7.4740	0.1719	0.3789	0.0087
5	0.393	71.11	4.4702	1.7568	0.3293	0.1294
6	0.001	106.56	14.5927	0.0146	0.3957	0.0004
7	0.245	62.36	3.1513	0.7721	0.6169	0.1511
8	0.001	96.91	10.5326	0.0105	0.4962	0.0005
9	0.233	77.87	5.6409	1.3143	0.4812	0.1121
10	0.046	49.63	1.8994	0.0874	0.5166	0.0238
<i>TEPL = 4.5201</i>					<i>TEVD = 0.4558</i>	

Table 8. The simulation results of the SORPD solution for TEPL reduction with WTs.

Scenario No.	σ_i	Loading %	Wind Speed (m/s)	P_w (MW)	P_{Loss} (MW)	EPL(MW)	EVD(p.u)	EVD(p.u)
1	0.011	42.10	5.04	11.747	1.3424	0.0148	0.3922	0.0043
2	0.027	91.46	8.38	31.032	5.9965	0.1619	0.4959	0.0134
3	0.02	78.61	15.57	72.496	2.5651	0.0513	0.4199	0.0084
4	0.023	85.30	13.36	59.762	3.7187	0.0855	0.7343	0.0169
5	0.393	71.11	7.72	27.238	2.8301	1.1122	0.4203	0.1652
6	0.001	106.56	9.42	37.034	12.4915	0.0125	0.2707	0.0003
7	0.245	62.36	10.37	42.543	1.5123	0.3705	0.4622	0.1132
8	0.001	96.91	14.40	65.779	4.9598	0.0050	0.4225	0.0004
9	0.233	77.87	5.70	15.581	4.4616	1.0396	0.5034	0.1173
10	0.046	49.63	8.93	34.184	1.0399	0.0478	0.3301	0.0152
$TEPL = 2.9011$							$TVED = 0.4546$	

In the case of solving the SORPD to reduce the TEVD without incorporating the WTs, the TEVD was decreased from 0.7919 p.u. to 4.5201 p.u. The voltage profile of the system at the base case is shown in Figure 11. The results of solving the SORPD without the insertion of WTs are recorded in Table 9. The voltage profile of the system was enhanced considerably, as shown in Figure 12, by solving the SORPD. The results of solving the SORPD with the insertion of WTs are recorded in Table 10. In the case of inclusion, the WTs, when solving the SORPD optimally with the TEVD, decreased from 0.7919 p.u. to 0.1249 p.u. compared to the base case. The simulation results are depicted in Table 10. The voltage profile, incorporating the WTs, is depicted in Figure 13, which verifies the enhancement of the voltage profile with the inclusion of WTs. The optimal values of the voltages are illustrated in Figures 12 and 13. The optimal values of the transformers’ tap ratios and the injected reactive powers for TEPL are listed in Appendix B in Tables A2 and A3, respectively. Likewise, the optimal values of the transformers’ tap ratios and the injected reactive powers for TEVD are listed in Appendix B in Tables A4 and A5, respectively.

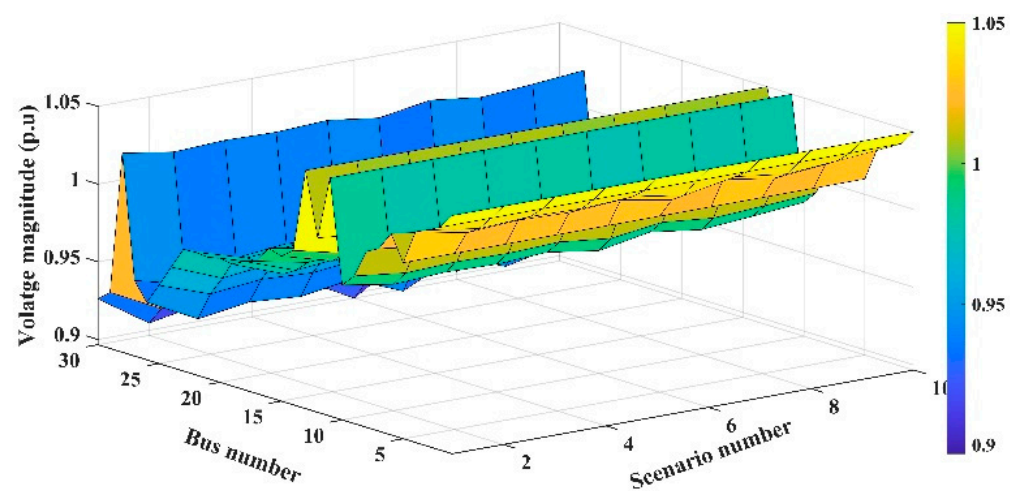


Figure 11. The voltage profile for the base case of the system.

Table 9. The simulation results of the SORPD solution for TEVD reduction without WTs.

Scenario No.	σ_i	Loading %	P_{Loss} (MW)	EPL(MW)	VD(p.u)	EVD(p.u)
1	0.011	42.10	2.3753	0.0261	0.2164	0.0024
2	0.027	91.46	10.7310	0.2897	0.2510	0.0068
3	0.02	78.61	6.5879	0.1318	0.2130	0.0043
4	0.023	85.30	9.2064	0.2117	0.2145	0.0049
5	0.393	71.11	5.2047	2.0455	0.1282	0.0504
6	0.001	106.56	13.4473	0.0134	0.2799	0.0003
7	0.245	62.36	4.1113	1.0073	0.1292	0.0317
8	0.001	96.91	12.3517	0.0124	0.6952	0.0007
9	0.233	77.87	6.7513	1.5730	0.1130	0.0263
10	0.046	49.63	4.1757	0.1921	0.1559	0.0072
<i>TEPL</i> = 5.5030					<i>TEVD</i> = 0.1349	

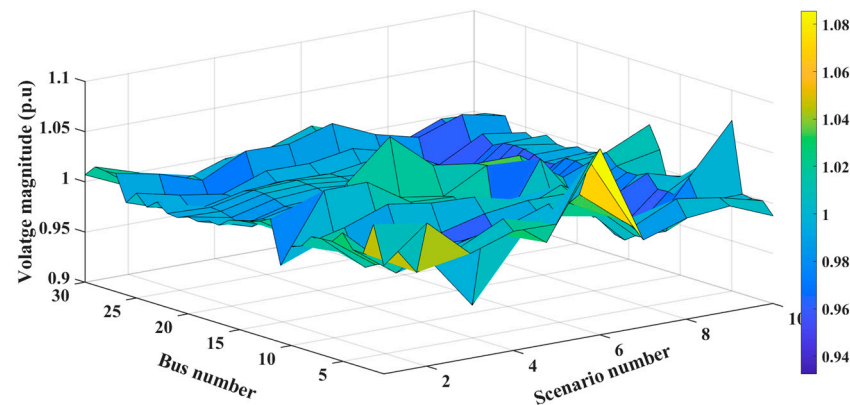


Figure 12. The system’s voltage profile without WTs.

Table 10. The simulation results of the SORPD solution for TEVD’s reduction with WTs.

Scenario NO.	σ_i	Loading %	Wind Speed (m/s)	P_w (MW)	P_{Loss} (MW)	EPL(MW)	EVD(p.u)	EVD(p.u)
1	0.011	0.011	42.10	2.3753	3.5862	0.0394	0.1599	0.0018
2	0.027	0.027	91.46	10.7310	6.2666	0.1692	0.2493	0.0067
3	0.02	0.02	78.61	6.5879	2.6767	0.0535	0.2026	0.0041
4	0.023	0.023	85.30	9.2064	3.8184	0.0878	0.1718	0.0040
5	0.393	0.393	71.11	5.2047	3.7606	1.4779	0.1075	0.0422
6	0.001	0.001	106.56	13.4473	10.5488	0.0105	0.5717	0.0006
7	0.245	0.245	62.36	4.1113	4.9506	1.2129	0.1163	0.0285
8	0.001	0.001	96.91	12.3517	5.4928	0.0055	0.1931	0.0002
9	0.233	0.233	77.87	6.7513	6.3825	1.4871	0.1354	0.0315
10	0.046	0.046	49.63	4.1757	1.1932	0.0549	0.1178	0.0054
<i>TEPL</i> = 4.5989					<i>TEVD</i> = 0.1249			

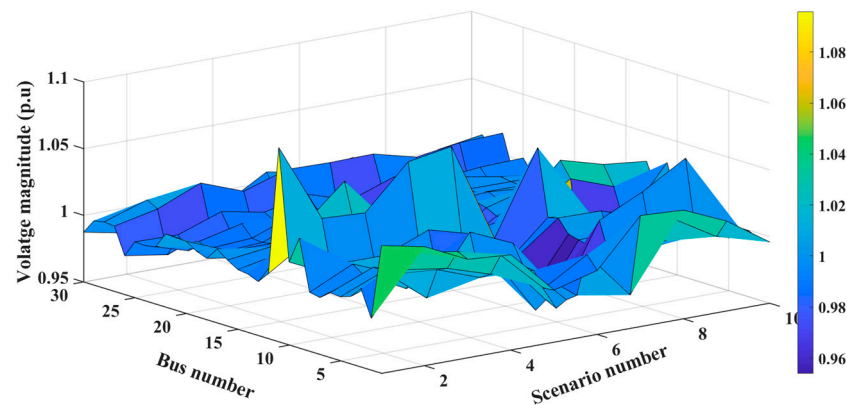


Figure 13. The system's voltage profile with WTs.

The unique features and findings of this paper can be summarized as follows:

- An Adaptive Manta-Ray Foraging Optimization (AMRFO) is proposed based on the quasi-oppositional based learning fitness distance balance method, which was successfully applied to solve the conventional and stochastic ORPD problem.
- The suggested AMRFO was validated on the standard benchmark functions compared to SCSO, WOA, GWO, AHA, DO, and the conventional MRFO in terms of the best, mean, worst and p -value.
- In the case of solving the conventional ORPD, the minimum power loss and the VD that was obtained by the application of the AMRFO were 4.5279 MW and 0.0913 p.u., respectively.
- The stochastic ORPD problem was solved by considering the uncertainties of the load demand and wind speed.
- The TEPL decreased from 5.1025 MW to 4.5201 MW in the case of solving the SORPD without the inclusion of WTs, while this value was reduced from 5.1025 MW to 2.9011 MW compared to the base case with the inclusion of WTs. Likewise, the TEVD decreased from 0.7919 p.u. to 0.1349 p.u. without incorporating the WTs, and this decreased from 0.7919 p.u. to 0.1249 p.u. with the inclusion of WTs compared with the base case.

The limitation of this work is that the proposed algorithm was implemented for the IEEE 30-bus system only without considering the energy storage systems. In this regard, the proposed technique should be applied to solve large-scale systems such as IEEE 57-bus and IEEE 30-bus with renewable energy and energy storage systems. In addition, the SORPD should be solved by considering network attacks such as false data injection (FDI) attacks [70] and denial of service (DoS) attacks [71].

6. Conclusions

This paper presented an efficient Adaptive Manta-Ray Foraging Optimization (AMRFO) to solve the conventional optimal reactive power dispatch (ORPD) and the stochastic optimal reactive power dispatch (SORPD). The AMRFO was based on enhancing the searching abilities and the exploration and exploitation phases of the standard Manta-Ray Foraging Optimization (MRFO) using three efficient improvement methods, including the Fitness distance Balance, the Quasi-Oppositional based learning (QOBL) and the adaptive Levy Flight (ALF). The normal and the Weibull PDFs, along with a Monte Carlo simulation and the scenario-based reduction method (SBR), were utilized to represent the uncertainties of the load demand and the produced power from the WTs to obtain a set of scenarios for the stochastic representation of uncertain parameters. In total, 1000 scenarios were obtained from the MCS, and by application, these scenarios were reduced to 10 scenarios. The suggested AMRFO was applied to 23 standard benchmark functions and on the IEEE 30-bus transmission system. The yielded results were compared to the conventional MRFO, SCSO, GWO, WOA, AHA, DO, and other well-known optimizers. The obtained results

revealed that the proposed AMFO was superior when solving the conventional ORPD and the stochastic ORPD compared to the other algorithms. In addition to this, the system's performance was enhanced considerably when solving the ORPD and the stochastic ORPD, especially with the inclusion of WTs in the system. The power loss was reduced by 19.09%, and the VD was reduced by 89.49% compared to the initial case of solving the conventional ORPD. Furthermore, the TEVD decreased by 82.97% and 84.23% through solving the SORPD without and with the inclusion of the WTs, respectively.

Author Contributions: Conceptualization, S.Z.A., E.A.M. and F.F.M.E.-S.; methodology, S.Z.A. and E.A.M.; software, S.Z.A., E.A.M. and F.F.M.E.-S.; validation, S.Z.A., E.A.M. and F.F.M.E.-S.; formal analysis, S.Z.A., E.A.M. and F.F.M.E.-S.; investigation, S.Z.A., E.A.M. and F.F.M.E.-S.; resources, E.A.M.; data curation, S.Z.A., E.A.M. and F.F.M.E.-S.; writing—original draft preparation, E.A.M.; writing—review and editing, S.Z.A., E.A.M. and F.F.M.E.-S.; visualization, S.Z.A. and F.F.M.E.-S.; supervision, F.F.M.E.-S.; project administration, S.Z.A. and F.F.M.E.-S.; funding acquisition, S.Z.A., E.A.M., and F.F.M.E.-S. All authors have read and agreed to the published version of the manuscript.

Funding: This project was funded by the Deanship of Scientific Research at Prince Sattam bin Abdulaziz University award number 2022/01/20089.

Institutional Review Board Statement: Not applicable.

Informed Consent Statement: Not applicable.

Data Availability Statement: Not applicable.

Conflicts of Interest: The authors declare no conflict of interest.

Abbreviations

ORPD	Optimal reactive power dispatch
AMRFO	Adaptive Manta-Ray Foraging Optimization
MRFO	Manta-Ray Foraging Optimization
SORPD	Stochastic ORPD
FDB	Fitness distance balance selection
ALF	An adaptive Levy Flight
QOBL	Quasi Oppositional based learning
MCS	The Monte Carlo simulation
PLoss	The power loss
TEPL	The total expected PLoss
VD	The voltage deviations
TEVD	The total expected VD
PDF	Probability density function
SCSO	Sand Cat Swarm algorithm
GWO	Grey Wolf Optimizer
WOA	Whale Optimization Algorithm technique
AHA	Artificial Hummingbird Algorithm
DO	Dandelion Optimizer
SBR	The scenario-based reduction
PSO	Particle Swarm Optimization
OBL	The Opposition-based learning
WT	Wind turbine
TLBO	Teach learning-based optimization
HPSO-TS	Hybrid PSO and Tabu search
MPA	Marine predator Algorithm
PSO-TVAC	PSO with time varying acceleration coefficients
CLPSO	Comprehensive Learning PSO
QOTLBO	Quasi Oppositional Teaching Learning based Optimization
JA	Jaya Algorithm

HSO	Harmony Search Algorithm
SGA	Standard Genetic Algorithm
DE	Differential Evolution
SpGA	Specialized Genetic Algorithm
FA	Firefly Algorithm
ALO	Ant Lion Optimizer
HPSO-TS	Hybrid PSO and Tabu search
TS	Tabu search
WOA	Whale Optimization Algorithm
IDE	Improved Differential Evolution
BBO	Biogeography-Based Optimization
CLPSO	Comprehensive Learning PSO
GSA	Gravitational Search Algorithm
GSA-CSS	GSA With Conditional Selection Strategies
IGSA-CSS	Improved GSA With Conditional Selection Strategies

Appendix A The Simulation Results for the Standard Objective Function

Table A1. Statistical results for the standard benchmark functions.

Fun	Algorithms	Average	Best	Worst	SD	p-Value	Mean Rank
F1	SCSO	1.7E−53	3.3E−61	3.8E−52	7.6E−53	9.73E−11	4
	GWO	6.4E−11	2.5E−12	3.31E−10	8.1E−11	9.73E−11	6
	WOA	9.7E−33	4.3E−43	7.21E−32	2.1E−32	9.73E−11	5
	AHA	8.1E−65	8.7E−82	1.81E−63	3.6E−64	9.73E−11	3
	DO	8.2E−03	3.3E−03	1.51E−02	3.6E−03	9.73E−11	5
	MRFO	1.7E−195	2.3E−215	3.41E−194	0.0E+00	9.73E−11	2
	AMRFO	0.0	0.0	0.0	0.0	-	1
F2	SCSO	5.51E−29	6.3E−34	4.5E−28	1.3E−28	1.37E−09	4
	GWO	3.61E−07	1.42E−07	7.71E−07	1.71E−07	1.38E−09	6
	WOA	4.30E−23	2.01E−27	6.61E−22	1.41E−22	1.37E−09	5
	AHA	1.50E−33	3.21E−40	2.9E−32	5.91E−33	1.37E−09	3
	DO	3.51E−02	1.11E−02	7.91E−02	1.51E−02	1.37E−09	7
	MRFO	2.51E−99	5.2E−108	6.21E−98	1.2E−98	1.37E−09	2
	AMRFO	0.0	0.0	0.0	0.0	-	1
F3	SCSO	2.91E−46	1.51E−55	6.91E−45	1.41E−45	9.73E−11	4
	GWO	1.51E+00	3.42E−02	2.11E+01	4.21E+0	9.73E−11	5
	WOA	8.12E+04	2.81E+04	1.21E+05	2.1E+04	9.73E−11	7
	AHA	3.01E−57	5.21E−72	7.42E−56	1.52E−56	9.73E−11	3
	DO	6.81E+02	1.12E+02	2.02E+03	5.4E+02	9.73E−11	6
	MRFO	6.72E−186	4.6E−200	1.71E−184	0	9.73E−11	2
	AMRFO	0	0	0	0	-	1

Table A1. Cont.

Fun	Algorithms	Average	Best	Worst	SD	p-Value	Mean Rank
F4	SCSO	1.22E−24	4.71E−28	2.42E−23	4.81E−24	1.42E−09	4
	GWO	1.31E−02	4.52E−03	4.71E−02	1.12E−02	1.42E−09	5
	WOA	5.81E+01	1.02E−05	9.02E+01	3.01E+01	1.42E−09	7
	AHA	7.82E−31	4.12E−38	1.61E−29	3.12E−30	1.42E−09	3
	DO	8.81E+00	2.31E+00	1.91E+01	4.92E+00	1.42E−09	6
	MRFO	2.60E−98	4.2E−106	3.41E−97	7.40E−98	1.42E−09	2
	AMRFO	0	0	0	0	-	1
F5	SCSO	2.83E+01	2.73E+01	2.93E+01	5.63E−01	1.42E−09	3
	GWO	2.83E+01	2.64E+01	2.94E+01	8.23E−01	1.42E−09	4
	WOA	2.92E+01	2.83E+01	2.93E+01	2.83E−01	1.42E−09	6
	AHA	2.83E+01	2.73E+01	2.92E+01	5.231E−01	1.42E−09	5
	DO	4.73E+01	2.53E+01	1.03E+02	2.73E+01	1.6E−09	7
	MRFO	2.53E+01	2.43E+01	2.62E+01	4.32E−01	4.1E−07	2
	AMRFO	2.41E+01	2.32E+01	2.60E+01	6.40E−01	-	1
F6	SCSO	2.52E+00	1.41E+00	3.31E+00	4.41E−01	1.42E−09	7
	GWO	1.31E+00	2.61E−01	2.02E+00	4.61E−01	1.42E−09	6
	WOA	1.3E+00	2.12E−01	1.91E+00	4.12E−01	1.42E−09	5
	AHA	1.02E+00	2.91E−01	1.81E+00	3.71E−01	1.42E−09	4
	DO	3.12E−03	6.61E−04	1.61E−02	3.71E−03	1.42E−09	3
	MRFO	1.61E−04	7.52E−06	1.13E−03	2.41E−04	4.46E−08	2
	AMRFO	9.52E−06	4.61E−07	4.91E−05	1.31E−05	-	1
F7	SCSO	5.913E−04	1.92E−05	2.43E−03	6.91E−04	2.66E−06	4
	GWO	5.91E−03	3.13E−03	1.43E−02	2.72E−03	1.42E−09	5
	WOA	7.81E−03	2.03E−04	4.22E−02	9.13E−03	1.42E−09	6
	AHA	5.13E−04	5.31E−05	1.22E−03	3.13E−04	2.57E−08	3
	DO	6.13E−02	2.03E−02	1.52E−01	3.61E−02	1.42E−09	7
	MRFO	3.81E−04	1.43E−05	1.23E−03	2.72E−04	2.2E−06	2
	AMRFO	7.61E−05	2.8E−06	1.71E−04	4.8E−05	-	1
F8	SCSO	−6.7E+03	−7.7E+03	−5.5E+03	6.4E+02	2.57E−09	4
	GWO	−6.4E+03	−7.6E+03	−3.5E+03	9.6E+02	1.6E−09	5
	WOA	−9.7E+03	−1.5E+04	−7.1E+03	2.13E+03	0.077453	6
	AHA	−9.9E+03	−1.4E+04	−9.2E+03	4.5E+02	7.38E−09	3
	DO	−7.7E+03	−8.5E+03	−5.6E+03	7.31E+02	8.55E−08	7
	MRFO	−7.7E+03	−9.2E+03	−6.6E+03	7.41E+02	0.002991	2
	AMRFO	−8.4E+03	−9.3E+03	−7.3E+03	5.27E+02	-	1

Table A1. Cont.

Fun	Algorithms	Average	Best	Worst	SD	p-Value	Mean Rank
F9	SCSO	0	0	0	0	N/A	1
	GWO	1.22E+01	1.12E+00	2.61E+01	7.71E+00	9.73E−11	6
	WOA	2.32E−15	0	5.72E−14	1.13E−14	0.337055	5
	AHA	0	0	0	0	N/A	2
	DO	5.61E+01	1.31E+01	1.42E+02	3.02E+01	9.73E−11	7
	MRFO	0	0	0	0	N/A	3
	AMRFO	0	0	0	0	-	4
F10	SCSO	8.92E−16	8.91E−16	8.91E−16	0	N/A	2
	GWO	1.42E−06	5.1E−07	3.91E−06	7.61E−07	9.73E−11	4
	WOA	1.02E−14	8.91E−16	2.22E−14	5.91E−15	2.74E−10	3
	AHA	8.91E−16	8.91E−16	8.91E−16	0	N/A	1
	DO	9.52E−02	1.32E−02	1.32E+00	2.61E−01	9.73E−11	5
	MRFO	8.91E−16	8.91E−16	8.91E−16	0	N/A	1
	AMRFO	8.91E−16	8.91E−16	8.91E−16	0	-	1
F11	SCSO	0	0	0	0	N/A	1
	GWO	1.13E−02	8.11E−12	4.72E−02	1.42E−02	9.73E−11	3
	WOA	4.62E−02	0	6.51E−01	1.63E−01	0.081168	5
	AHA	0	0	0	0	N/A	2
	DO	3.61E−02	6.02E−03	9.81E−02	2.21E−02	9.73E−11	4
	MRFO	0	0	0	0	N/A	2
	AMRFO	0	0	0	0	N/A	2
F12	SCSO	1.32E−01	2.61E−02	3.33E−01	6.12E−02	4.13E−09	6
	GWO	8.31E−02	3.22E−02	1.81E−01	3.61E−02	1.46E−08	5
	WOA	8.13E−02	1.33E−02	2.52E−01	5.72E−02	1.31E−08	4
	AHA	2.63E−02	2.72E−03	8.22E−02	1.81E−02	2.57E−08	3
	DO	4.92E−01	4.12E−05	2.71E+00	8.12E−01	7.38E−09	7
	MRFO	6.61E−06	3.62E−07	2.63E−05	6.91E−06	8.86E−06	1
	AMRFO	4.12E−03	1.33E−08	1.02E−01	2.13E−02	-	2
F13	SCSO	2.41E+00	1.42E+00	2.91E+00	4.02E−01	0.006223	5
	GWO	1.12E+00	6.31E−01	1.61E+00	3.02E−01	3.7E−07	2
	WOA	1.13E+00	3.02E−01	2.13E+00	4.41E−01	7.51E−07	3
	AHA	2.31E+00	1.51E−01	2.91E+00	6.01E−01	0.00384	4
	DO	4.41E−02	2.41E−04	5.31E−01	1.11E−01	1.8E−09	1
	MRFO	2.51E+00	1.41E−02	3.01E+00	1.01E+00	0.004614	6
	AMRFO	2.51E+00	3.01E−01	3.01E+00	7.81E−01	-	6

Table A1. Cont.

Fun	Algorithms	Average	Best	Worst	SD	p-Value	Mean Rank
F14	SCSO	4.23E+00	1.02E+00	1.31E+01	4.42E+00	1.38E−10	5
	GWO	5.51E+00	1.02E+00	1.31E+01	4.60E+00	1.38E−10	7
	WOA	4.41E+00	1.02E+00	1.11E+01	3.61E+00	1.38E−10	6
	AHA	1.23E+00	1.02E+00	3.02E+00	6.71E−01	1.83E−10	3
	DO	1.43E+00	1.02E+00	3.02E+00	7.31E−01	1.37E−10	4
	MRFO	1.01E+00	1.02E+00	1.02E+00	1.72E−16	7.52E−05	2
	AMRFO	1.0E+00	1.02E+00	1.02E+00	4.51E−17	-	1
F15	SCSO	5.21E−04	3.11E−04	1.21E−03	2.61E−04	1.42E−09	3
	GWO	3.01E−03	3.61E−04	2.01E−02	6.61E−03	1.42E−09	6
	WOA	1.31E−03	3.31E−04	1.71E−02	3.31E−03	1.42E−09	5
	AHA	3.12E−04	3.12E−04	3.41E−04	7.21E−06	1.42E−09	2
	DO	4.71E−03	3.12E−04	2.02E−02	8.01E−03	1.42E−09	7
	MRFO	1.22E−03	3.12E−04	2.02E−02	4.01E−03	1.42E−09	4
	AMRFO	3.10E−04	3.10E−04	3.11E−04	9.34E−15	-	1
F16	SCSO	−1.0E+00	−1.0E+00	−1.0E+00	3.92E−09	1.87E−10	1
	GWO	−1.0E+00	−1.0E+00	−1.0E+00	2.52E−07	1.87E−10	1
	WOA	−1.0E+00	−1.0E+00	−1.0E+00	9.22E−08	1.87E−10	1
	AHA	−1.0E+00	−1.0E+00	−1.0E+00	3.91E−12	8.8E−09	1
	DO	−1.0E+00	−1.0E+00	−1.0E+00	2.33E−11	1.87E−10	1
	MRFO	−1.0E+00	−1.0E+00	−1.0E+00	6.11E−16	0.018662	1
	AMRFO	−1.0E+00	−1.0E+00	−1.0E+00	6.61E−16	-	1
F17	SCSO	4.0E−01	4.0E−01	4.0E−01	3.71E−07	9.73E−11	1
	GWO	4.0E−01	4.0E−01	4.0E−01	2.81E−06	9.73E−11	1
	WOA	4.0E−01	4.0E−01	4.0E−01	1.41E−04	9.73E−11	1
	AHA	4.0E−01	4.0E−01	4.0E−01	0	N/A	1
	DO	4.0E−01	4.0E−01	4.0E−01	2.91E−10	9.73E−11	1
	MRFO	4.0E−01	4.0E−01	4.0E−01	0	N/A	1
	AMRFO	4.0E−01	4.0E−01	4.0E−01	0	-	1
F18	SCSO	3.02E+00	3.02E+00	3.02E+00	3.62E−05	1.24E−09	1
	GWO	3.02E+00	3.02E+00	3.02E+00	3.42E−04	1.24E−09	1
	WOA	3.02E+00	3.02E+00	3.02E+00	1.51E−03	1.24E−09	1
	AHA	3.02E+00	3.02E+00	3.02E+00	2.02E−15	0.483014	1
	DO	3.02E+00	3.02E+00	3.02E+00	1.13E−07	1.24E−09	1
	MRFO	3.02E+00	3.02E+00	3.02E+00	1.51E−15	0.052141	1
	AMRFO	3.02E+00	3.02E+00	3.02E+00	1.51E−15	-	1

Table A1. Cont.

Fun	Algorithms	Average	Best	Worst	SD	p-Value	Mean Rank
F19	SCSO	-3.8E+00	-3.8E+00	-3.8E+00	3.1E-03	1.87E-10	1
	GWO	-3.8E+00	-3.9E+00	-3.8E+00	2.5E-03	1.87E-10	1
	WOA	-3.7E+00	-3.8E+00	-3.6E+00	4.11E-02	1.87E-10	1
	AHA	-3.8E+00	-3.8E+00	-3.8E+00	5.82E-15	3.69E-08	1
	DO	-3.8E+00	-3.8E+00	-3.8E+00	1.1E-06	1.87E-10	1
	MRFO	-3.8E+00	-3.8E+00	-3.8E+00	2.3E-15	0.232368	1
	AMRFO	-3.9E+00	-3.9E+00	-3.9E+00	2.13E-15	-	1
F20	SCSO	-3.3E+00	-3.3E+00	-2.81E+00	1.12E-01	0.044224	1
	GWO	-3.3E+00	-3.3E+00	-3.12E+00	8.11E-02	0.144383	1
	WOA	-3.2E+00	-3.3E+00	-3.1E+00	1.23E-01	0.010339	1
	AHA	-3.3E+00	-3.3E+00	-3.21E+00	3.92E-02	0.937112	1
	DO	-3.3E+00	-3.3E+00	-3.22E+00	3.92E-02	0.937112	1
	MRFO	-3.3E+00	-3.3E+00	-3.21E+00	6.1E-02	0.407218	1
	AMRFO	-3.3E+00	-3.3E+00	-3.20E+00	6.0E-02	-	1
F21	SCSO	-5.2E+00	-1.0E+01	-8.7E-01	1.31E+00	7.19E-10	7
	GWO	-8.9E+00	-1.0E+01	-2.6E+00	2.51E+00	7.19E-10	3
	WOA	-7.4E+00	-1.0E+01	-2.5E+00	3.01E+00	7.19E-10	5
	AHA	-9.4E+00	-1.0E+01	-4.9E+00	1.91E+00	7.19E-10	2
	DO	-7.3E+00	-1.0E+01	-2.6E+00	3.51E+00	7.19E-10	6
	MRFO	-7.8E+00	-1.0E+01	E+00	2.61E+00	9.48E-05	4
	AMRFO	-1.0E+01	-1.0E+01	-1.0E+01	4.40E-15	-	1
F22	SCSO	-6.2E+00	-1.0E+01	-9.3E-01	2.62E+00	6.34E-09	6
	GWO	-1.0E+01	-1.0E+01	-5.3E+00	1.12E+00	7.15E-09	1
	WOA	-6.6E+00	-1.0E+01	-2.1E+00	3.22E+00	3.91E-09	5
	AHA	-9.6E+00	-1.0E+01	-5.3E+00	1.92E+00	7.15E-09	3
	DO	-61+00	-1.0E+01	-1.9E+00	3.52E+00	1.65E-09	7
	MRFO	-7.2E+00	-1.0E+01	-2.9E+00	2.82E+00	3.66E-05	4
	AMRFO	-1.0E+01	-1.0E+01	-3.8E+00	1.31E+00	-	2
F23	SCSO	-6.1E+00	-1.1E+01	-2.91E+00	2.42E+00	7.54E-10	6
	GWO	-1.0E+01	-1.1E+01	-2.51E+00	1.61E+00	7.54E-10	2
	WOA	-5.8E+00	-1.1E+01	-1.81E+00	2.91E+00	7.54E-10	7
	AHA	-9.9E+00	-1.1E+01	-5.31E+00	1.72E+00	7.54E-10	3
	DO	-7.6E+00	-1.1E+01	-2.51E+00	3.62E+00	7.54E-10	5
	MRFO	-8.3E+00	-1.1E+01	-3.91E+00	2.91E+00	1.05E-05	4
	AMRFO	-1.1E+01	-1.1E+01	-1.11E+01	2.81E-15	-	1

Appendix B The Optimal Control Variables for Solving the SORPD

Table A2. The optimal tap setting of transformers with and without WTs for TEPL reduction.

Without Incorporating WTs				
Scenario No.	T11	T12	T15	T36
1	1.02	0.99	0.97	1.03
2	1.02	1.05	1.05	1.02
3	0.98	1.04	1	0.96
4	1.06	0.97	1.04	1
5	1	1.07	1.04	1.02
6	0.97	1.03	1.04	0.99
7	0.95	1.01	1.02	0.99
8	0.99	1	1.05	1.05
9	1.01	1.01	1.03	1.01
10	1.01	1.04	1.04	1.08
Incorporating WTs				
Scenario No.	T11	T12	T15	T36
1	1.01	1.03	1.05	0.98
2	1	1.04	0.98	0.99
3	1.04	0.98	1.01	0.97
4	1.08	1.04	1.07	1.05
5	1.03	0.97	1.01	1.01
6	1.02	0.97	1.02	0.98
7	0.97	0.99	1.01	0.99
8	1.02	1.06	0.99	0.97
9	1.07	0.93	0.97	1.01
10	1.01	1.06	1.01	1

Table A3. The optimal injected reactive powers by capacitors with and without WTs for TEPL reduction.

Without Incorporating WTs									
Scenario No.	Q10	Q12	Q15	Q17	Q20	Q21	Q23	Q24	Q29
1	1.86	2.49	1.82	2.49	1.34	1.63	2.76	2.6	2.04
2	3.36	1.73	3.18	2.12	3.29	1.8	1.67	1.56	3.15
3	1.17	3.61	2.85	1.82	1.21	2.15	2.62	1.47	3.06
4	3.38	1.97	3	3.01	2.53	0.35	3.37	1.84	2.43
5	1.38	2.52	1.89	3.67	3.82	2.76	2.39	4	4.16
6	2.88	1.94	3.24	2.79	1.86	2.17	1.33	2.73	2.69
7	1.58	1.25	2.21	3.17	1.47	3.17	0.89	2.95	1.2
8	1.85	3.14	2.52	3.19	2.26	3.49	2.04	2.22	3.33
9	3.78	0.85	2.87	1.93	2.88	3.91	4.01	1.63	3.39
10	3.27	2.29	2.59	1.81	2.88	2.09	1.61	4.45	3.22
Incorporating WTs									
Scenario No.	Q10	Q12	Q15	Q17	Q20	Q21	Q23	Q24	Q29
1	3.95	3.28	2.83	2.39	1.49	1.33	2.55	2.98	2.15
2	2.34	1.86	2.92	1.74	2.79	4.02	3.46	2.67	2.27
3	0.49	1.2	3.41	3.83	2.51	1.31	4.1	1.23	3.68
4	1.61	3.37	3.72	2.06	2.79	1.97	2.26	3.54	3.2
5	2.68	2.6	3.21	1.81	4.33	2.97	1.74	2.29	4.41
6	2.05	2.23	2.34	2.18	2.46	3.64	2.8	1.43	2.81
7	1.54	3.95	4.27	2.91	2.64	2.92	2.69	2.5	2.16
8	3.8	3.38	3.05	2.38	3.39	4.05	2.93	0.87	2.37
9	1.83	2.18	3.23	2.88	2.15	3.31	2.84	3.72	2.59
10	1.85	3.97	0.44	4.5	4.1	3.58	2.59	2.32	3.99

Table A4. The optimal taps setting of transformers with and without WTs for TEVD reduction.

Without Incorporating WTs				
Scenario No.	T11	T12	T15	T36
1	0.96	0.96	1	0.97
2	1	1.04	1.02	0.95
3	1.03	0.93	0.99	0.97
4	1.01	0.94	1	0.94
5	1.03	0.91	0.96	0.97
6	0.99	1.06	0.98	0.96
7	1	0.96	1.01	0.96
8	0.94	0.94	0.98	1.01
9	1.02	1	0.99	0.97
10	0.93	1.01	1.02	0.98
Incorporating WTs				
Scenario No.	T11	T12	T15	T36
1	1.01	1.01	0.91	1
2	1.01	1.02	0.95	0.96
3	0.99	0.92	0.98	0.97
4	1	0.94	1	0.96
5	0.97	0.95	0.98	0.98
6	1.03	0.99	0.94	0.98
7	0.98	1.01	1.02	0.96
8	0.96	0.96	0.99	0.92
9	0.96	0.98	0.99	0.95
10	0.98	0.96	1	0.99

Table A5. The optimal injected reactive powers by capacitors with and without WTs for TEVD reduction.

Without Incorporating WTs									
Scenario No.	Q10	Q12	Q15	Q17	Q20	Q21	Q23	Q24	Q29
1	3.86	2.05	3.33	4.13	4.67	3.16	3.92	2.36	2.42
2	1.29	3.74	1.72	2.97	2.61	3.18	2.3	4.2	3.42
3	1.81	1.96	2.68	1.82	1.39	2.05	2.66	1.97	3.4
4	2.29	0.79	2.23	2.15	2.69	3.08	1.59	2.56	3.41
5	2.46	1.09	1.52	2.72	1.7	2.71	3.07	3.29	3.12
6	3.4	1.7	3.02	2.22	1.86	3.68	2.76	1.62	2.46
7	2.5	2.4	2.23	4.14	2.92	2.1	1.04	3.03	1.91
8	3.59	1.96	3.3	1.32	3.51	2.96	1.41	1.4	3.01
9	3.69	2.05	2.09	3.33	4.09	2.37	3.47	1.69	4.32
10	3.44	4.01	3.04	0.76	2.52	2.87	2.63	2.68	3.41
Incorporating WTs									
Scenario No.	Q10	Q12	Q15	Q17	Q20	Q21	Q23	Q24	Q29
1	1.97	3.17	1.7	0.73	2.47	1.33	2.14	3	2.32
2	1.79	1.58	4.3	3.7	3.94	1.32	1.35	2.99	3.7
3	1.71	2.64	2.69	2.71	1.69	2.85	2.05	3.87	3.74
4	3.03	4.27	3.09	1.81	2.9	2.71	1.53	2.24	1.88
5	2.23	2.44	3.35	2.46	2.07	1.8	3.12	3.94	3.82
6	3.61	2.75	3.02	2.97	2.26	1.44	2.16	1.65	2.8
7	3.43	1.71	3.81	2.01	2.54	2.2	0.87	2.48	2.95
8	2.64	2.29	2.66	2.42	2.42	3.25	2.78	2.14	4.32
9	3	2.76	1.41	2	4.73	3.74	3.39	3.31	1.62
10	2.11	1.99	1.73	1.54	1.67	2.35	2.38	3.34	2.96

References

1. Wu, Q.; Cao, Y.; Wen, J. Optimal reactive power dispatch using an adaptive genetic algorithm. *Int. J. Electr. Power Energy Syst.* **1998**, *20*, 563–569. [[CrossRef](#)]
2. Wu, Q.H.; Ma, J. Power system optimal reactive power dispatch using evolutionary programming. *IEEE Trans. Power Syst.* **1995**, *10*, 1243–1249. [[CrossRef](#)] [[PubMed](#)]
3. Dai, C.; Chen, W.; Zhu, Y.; Zhang, X. Seeker optimization algorithm for optimal reactive power dispatch. *IEEE Trans. Power Syst.* **2009**, *24*, 1218–1231.
4. Granville, S. Optimal reactive dispatch through interior point methods. *IEEE Trans. Power Syst.* **1994**, *9*, 136–146. [[CrossRef](#)]
5. Lee, K.; Park, Y.; Ortiz, J. A united approach to optimal real and reactive power dispatch. *IEEE Trans. Power Appar. Syst.* **1985**, *PAS-104*, 1147–1153. [[CrossRef](#)]
6. Terra, L.; Short, M. Security-constrained reactive power dispatch. *IEEE Trans. Power Syst.* **1991**, *6*, 109–117. [[CrossRef](#)]
7. Quintana, V.; Santos-Nieto, M. Reactive-power dispatch by successive quadratic programming. *IEEE Trans. Energy Convers.* **1989**, *4*, 425–435. [[CrossRef](#)]
8. Abou El Ela, A.; Abido, M.; Spea, S. Differential evolution algorithm for optimal reactive power dispatch. *Electr. Power Syst. Res.* **2011**, *81*, 458–464. [[CrossRef](#)]
9. Zhao, B.; Guo, C.; Cao, Y. A multiagent-based particle swarm optimization approach for optimal reactive power dispatch. *IEEE Trans. Power Syst.* **2005**, *20*, 1070–1078. [[CrossRef](#)]
10. Kamel, S.; Abdel-Fatah, S.; Ebeed, M.; Yu, J.; Xie, K.; Zhao, C. Solving optimal reactive power dispatch problem considering load uncertainty. In Proceedings of the 2019 IEEE Innovative Smart Grid Technologies-Asia (ISGT Asia), Chengdu, China, 21–24 May 2019; pp. 1335–1340.
11. Abdel-Fatah, S.; Ebeed, M.; Kamel, S.; Nasrat, L. Moth swarm algorithm for reactive power dispatch considering stochastic nature of renewable energy generation and load. In Proceedings of the 2019 21st International Middle East Power Systems Conference (MEPCON), Cairo, Egypt, 17–19 December 2019; pp. 594–599.
12. Villa-Acevedo, W.M.; López-Lezama, J.M.; Valencia-Velásquez, J.A. A novel constraint handling approach for the optimal reactive power dispatch problem. *Energies* **2018**, *11*, 2352. [[CrossRef](#)]
13. Li, Z.; Cao, Y.; Dai, L.V.; Yang, X.; Nguyen, T.T. Finding solutions for optimal reactive power dispatch problem by a novel improved antlion optimization algorithm. *Energies* **2019**, *12*, 2968. [[CrossRef](#)]
14. Abido, M.A. Multiobjective optimal VAR dispatch using strength pareto evolutionary algorithm. In Proceedings of the 2006 IEEE International Conference on Evolutionary Computation, Vancouver, BC, Canada, 16–21 July 2006; pp. 730–736.
15. Nguyen, T.T.; Vo, D.N. Improved social spider optimization algorithm for optimal reactive power dispatch problem with different objectives. *Neural Comput. Appl.* **2019**, *32*, 5919–5950. [[CrossRef](#)]
16. Prasad, D.; Banerjee, A.; Singh, R.P. Optimal Reactive Power Dispatch Using Modified Differential Evolution Algorithm. In *Advances in Computer, Communication and Control*; Springer: Singapore, 2019; pp. 275–283.
17. Ben oualid Medani, K.; Sayah, S.; Bekrar, A. Whale optimization algorithm based optimal reactive power dispatch: A case study of the Algerian power system. *Electr. Power Syst. Res.* **2018**, *163*, 696–705. [[CrossRef](#)]
18. Mouassa, S.; Bouktir, T.; Salhi, A. Ant lion optimizer for solving optimal reactive power dispatch problem in power systems. *Eng. Sci. Technol. Int. J.* **2017**, *20*, 885–895. [[CrossRef](#)]
19. Mahadevan, K.; Kannan, P. Comprehensive learning particle swarm optimization for reactive power dispatch. *Appl. Soft Comput.* **2010**, *10*, 641–652. [[CrossRef](#)]
20. Faramarzi, A.; Heidarinejad, M.; Mirjalili, S.; Gandomi, A.H. Marine Predators Algorithm: A nature-inspired metaheuristic. *Expert Syst. Appl.* **2020**, *152*, 113377. [[CrossRef](#)]
21. Heidari, A.A.; Abbaspour, R.A.; Jordehi, A.R. Gaussian bare-bones water cycle algorithm for optimal reactive power dispatch in electrical power systems. *Appl. Soft Comput.* **2017**, *57*, 657–671. [[CrossRef](#)]
22. Bhattacharya, A.; Chattopadhyay, P.K. Solution of optimal reactive power flow using biogeography-based optimization. *Int. J. Electr. Electron. Eng.* **2010**, *4*, 568–576.
23. Abdel-Fatah, S.; Ebeed, M.; Kamel, S. Optimal reactive power dispatch using modified sine cosine algorithm. In Proceedings of the 2019 International Conference on Innovative Trends in Computer Engineering (ITCE), Aswan, Egypt, 2–4 February 2019; pp. 510–514.
24. Khazali, A.; Kalantar, M. Optimal reactive power dispatch based on harmony search algorithm. *Int. J. Electr. Power Energy Syst.* **2011**, *33*, 684–692. [[CrossRef](#)]
25. Abdel-Fatah, S.; Ebeed, M.; Kamel, S.; Yu, J. Reactive Power Dispatch Solution with Optimal Installation of Renewable Energy Resources Considering Uncertainties. In Proceedings of the 2019 IEEE Conference on Power Electronics and Renewable Energy (CPERE), Aswan, Egypt, 23–25 October 2019; pp. 118–123.
26. Mandal, B.; Roy, P.K. Optimal reactive power dispatch using quasi-oppositional teaching learning based optimization. *Int. J. Electr. Power Energy Syst.* **2013**, *53*, 123–134. [[CrossRef](#)]
27. Chen, G.; Liu, L.; Zhang, Z.; Huang, S. Optimal reactive power dispatch by improved GSA-based algorithm with the novel strategies to handle constraints. *Appl. Soft Comput.* **2017**, *50*, 58–70. [[CrossRef](#)]
28. Duman, S.; Sönmez, Y.; Güvenc, U.; Yörükeren, N. Optimal reactive power dispatch using a gravitational search algorithm. *IET Gener. Transm. Distrib.* **2012**, *6*, 563–576. [[CrossRef](#)]

29. Wei, Y.; Zhou, Y.; Luo, Q.; Deng, W. Optimal reactive power dispatch using an improved slime mould algorithm. *Energy Rep.* **2021**, *7*, 8742–8759. [[CrossRef](#)]
30. Sahli, Z.; Hamouda, A.; Bekrar, A.; Trentesaux, D. Reactive power dispatch optimization with voltage profile improvement using an efficient hybrid algorithm. *Energies* **2018**, *11*, 2134. [[CrossRef](#)]
31. Shaheen, M.A.; Hasanien, H.M.; Alkuhayli, A. A novel hybrid GWO-PSO optimization technique for optimal reactive power dispatch problem solution. *Ain Shams Eng. J.* **2021**, *12*, 621–630. [[CrossRef](#)]
32. Khan, N.H.; Wang, Y.; Tian, D.; Jamal, R.; Ebeed, M.; Deng, Q. Fractional PSO-GSA algorithm approach to solve optimal reactive power dispatch problems with uncertainty of renewable energy resources. *IEEE Access* **2020**, *8*, 215399–215413. [[CrossRef](#)]
33. Khan, N.H.; Jamal, R.; Ebeed, M.; Kamel, S.; Zeinoddini-Meymand, H.; Zawbaa, H.M. Adopting Scenario-Based approach to solve optimal reactive power Dispatch problem with integration of wind and solar energy using improved Marine predator algorithm. *Ain Shams Eng. J.* **2022**, *13*, 101726. [[CrossRef](#)]
34. Ebeed, M.; Ali, A.; Mosaad, M.I.; Kamel, S. An improved lightning attachment procedure optimizer for optimal reactive power dispatch with uncertainty in renewable energy resources. *IEEE Access* **2020**, *8*, 168721–168731. [[CrossRef](#)]
35. Mohseni-Bonab, S.M.; Rabiee, A.; Mohammadi-Ivatloo, B.; Jalilzadeh, S.; Nojavan, S. A two-point estimate method for uncertainty modeling in multi-objective optimal reactive power dispatch problem. *Int. J. Electr. Power Energy Syst.* **2016**, *75*, 194–204. [[CrossRef](#)]
36. Naidji, M.; Boudour, M. Stochastic multi-objective optimal reactive power dispatch considering load and renewable energy sources uncertainties: A case study of the Adrar isolated power system. *Int. Trans. Electr. Energy Syst.* **2020**, *30*, e12374. [[CrossRef](#)]
37. Zhao, W.; Zhang, Z.; Wang, L. Manta ray foraging optimization: An effective bio-inspired optimizer for engineering applications. *Eng. Appl. Artif. Intell.* **2020**, *87*, 103300. [[CrossRef](#)]
38. Hassan, M.H.; Houssein, E.H.; Mahdy, M.A.; Kamel, S. An improved manta ray foraging optimizer for cost-effective emission dispatch problems. *Eng. Appl. Artif. Intell.* **2021**, *100*, 104155. [[CrossRef](#)]
39. Houssein, E.H.; Emam, M.M.; Ali, A.A. Improved manta ray foraging optimization for multi-level thresholding using COVID-19 CT images. *Neural Comput. Appl.* **2021**, *33*, 16899–16919. [[CrossRef](#)] [[PubMed](#)]
40. Bastawy, M.; Ebeed, M.; Ali, A.; Shaaban, M.F.; Khan, B.; Kamel, S. Optimal day-ahead scheduling in micro-grid with renewable based DGs and smart charging station of EVs using an enhanced manta-ray foraging optimisation. *IET Renew. Power Gener.* **2022**, *16*, 2413–2428. [[CrossRef](#)]
41. Tang, A.; Zhou, H.; Han, T.; Xie, L. A modified manta ray foraging optimization for global optimization problems. *IEEE Access* **2021**, *9*, 128702–128721. [[CrossRef](#)]
42. Shaheen, A.M.; El-Sehiemy, R.A.; Alharthi, M.M.; Ghoneim, S.S.; Ginidi, A.R. Multi-objective jellyfish search optimizer for efficient power system operation based on multi-dimensional OPF framework. *Energy* **2021**, *237*, 121478. [[CrossRef](#)]
43. Soroudi, A.; Aien, M.; Ehsan, M. A probabilistic modeling of photo voltaic modules and wind power generation impact on distribution networks. *IEEE Syst. J.* **2011**, *6*, 254–259. [[CrossRef](#)]
44. Khatod, D.K.; Pant, V.; Sharma, J. Evolutionary programming based optimal placement of renewable distributed generators. *IEEE Trans. Power Syst.* **2012**, *28*, 683–695. [[CrossRef](#)]
45. Hetzer, J.; David, C.Y.; Bhattarai, K. An economic dispatch model incorporating wind power. *IEEE Trans. Energy Convers.* **2008**, *23*, 603–611. [[CrossRef](#)]
46. Binder, K.; Heermann, D.; Roelofs, L.; Mallinckrodt, A.J.; McKay, S. Monte Carlo simulation in statistical physics. *Comput. Phys.* **1993**, *7*, 156–157. [[CrossRef](#)]
47. Mohseni-Bonab, S.M.; Rabiee, A.; Mohammadi-Ivatloo, B. Voltage stability constrained multi-objective optimal reactive power dispatch under load and wind power uncertainties: A stochastic approach. *Renew. Energy* **2016**, *85*, 598–609. [[CrossRef](#)]
48. Seguro, J.; Lambert, T. Modern estimation of the parameters of the Weibull wind speed distribution for wind energy analysis. *J. Wind. Eng. Ind. Aerodyn.* **2000**, *85*, 75–84. [[CrossRef](#)]
49. Grove-Kuska, N.; Heitsch, H.; Romisch, W. Scenario reduction and scenario tree construction for power management problems. In Proceedings of the 2003 IEEE Bologna Power Tech Conference Proceedings, Bologna, Italy, 23–26 June 2003; Volume 3, p. 7.
50. Biswas, P.P.; Suganthan, P.N.; Mallipeddi, R.; Amaratunga, G.A. Optimal reactive power dispatch with uncertainties in load demand and renewable energy sources adopting scenario-based approach. *Appl. Soft Comput.* **2019**, *75*, 616–632. [[CrossRef](#)]
51. Kahraman, H.T.; Aras, S.; Gedikli, E. Fitness-distance balance (FDB): A new selection method for meta-heuristic search algorithms. *Knowl.-Based Syst.* **2020**, *190*, 105169. [[CrossRef](#)]
52. Alkayem, N.F.; Shen, L.; Al-hababi, T.; Qian, X.; Cao, M. Inverse Analysis of Structural Damage Based on the Modal Kinetic and Strain Energies with the Novel Oppositional Unified Particle Swarm Gradient-Based Optimizer. *Appl. Sci.* **2022**, *12*, 11689. [[CrossRef](#)]
53. Yuan, P.; Zhang, T.; Yao, L.; Lu, Y.; Zhuang, W. A Hybrid Golden Jackal Optimization and Golden Sine Algorithm with Dynamic Lens-Imaging Learning for Global Optimization Problems. *Appl. Sci.* **2022**, *12*, 9709. [[CrossRef](#)]
54. Rao, R.V.; Rai, D.P. Optimization of submerged arc welding process parameters using quasi-oppositional based Jaya algorithm. *J. Mech. Sci. Technol.* **2017**, *31*, 2513–2522. [[CrossRef](#)]
55. Kandan, M.; Krishnamurthy, A.; Selvi, S.A.M.; Sikkandar, M.Y.; Aboamer, M.A.; Tamilvizhi, T. Quasi oppositional Aquila optimizer-based task scheduling approach in an IoT enabled cloud environment. *J. Supercomput.* **2022**, *78*, 10176–10190. [[CrossRef](#)]

56. Seyyedabbasi, A.; Kiani, F. Sand Cat swarm optimization: A nature-inspired algorithm to solve global optimization problems. *Eng. Comput.* **2022**. [[CrossRef](#)]
57. Mirjalili, S.; Mirjalili, S.M.; Lewis, A. Grey wolf optimizer. *Adv. Eng. Softw.* **2014**, *69*, 46–61. [[CrossRef](#)]
58. Mirjalili, S.; Lewis, A. The whale optimization algorithm. *Adv. Eng. Softw.* **2016**, *95*, 51–67. [[CrossRef](#)]
59. Zhao, W.; Wang, L.; Mirjalili, S. Artificial hummingbird algorithm: A new bio-inspired optimizer with its engineering applications. *Comput. Methods Appl. Mech. Eng.* **2022**, *388*, 114194. [[CrossRef](#)]
60. Zhao, S.; Zhang, T.; Ma, S.; Chen, M. Dandelion Optimizer: A nature-inspired metaheuristic algorithm for engineering applications. *Eng. Appl. Artif. Intell.* **2022**, *114*, 105075. [[CrossRef](#)]
61. Ebeed, M.; Ahmed, D.; Kamel, S.; Jurado, F.; Shaaban, M.F.; Ali, A.; Refai, A. Optimal energy planning of multi-microgrids at stochastic nature of load demand and renewable energy resources using a modified Capuchin Search Algorithm. *Neural Comput. Appl.* **2023**, 1–26. [[CrossRef](#)]
62. Jamil, M.; Yang, X.-S. A literature survey of benchmark functions for global optimization problems. *arXiv* **2013**, arXiv:1308.4008.
63. Molga, M.; Smutnicki, C. Test functions for optimization needs. *Test Funct. Optim. Needs* **2005**, *101*, 48.
64. IEEE 30-bus test system Data, I.-B.T.S. Available online: http://labs.ece.uw.edu/pstca/pf30/pg_tca30bus.htm (accessed on 29 May 2023).
65. Taher, S.A.; Amooshahi, M.K. New approach for optimal UPFC placement using hybrid immune algorithm in electric power systems. *Int. J. Electr. Power Energy Syst.* **2012**, *43*, 899–909. [[CrossRef](#)]
66. Mandal, S.; Mandal, K.; Kumar, S. A new optimization technique for optimal reactive power scheduling using Jaya algorithm. In Proceedings of the 2017 Innovations in Power and Advanced Computing Technologies (i-PACT), Vellore, India, 21–22 April 2017; pp. 1–5.
67. Rajan, A.; Malakar, T. Optimal reactive power dispatch using hybrid Nelder–Mead simplex based firefly algorithm. *Int. J. Electr. Power Energy Syst.* **2015**, *66*, 9–24. [[CrossRef](#)]
68. Ebeed, M.; Alhejji, A.; Kamel, S.; Jurado, F. Solving the optimal reactive power dispatch using marine predators algorithm considering the uncertainties in load and wind-solar generation systems. *Energies* **2020**, *13*, 4316. [[CrossRef](#)]
69. Polprasert, J.; Ongsakul, W.; Dieu, V.N. Optimal reactive power dispatch using improved pseudo-gradient search particle swarm optimization. *Electr. Power Compon. Syst.* **2016**, *44*, 518–532. [[CrossRef](#)]
70. Li, F.; Li, K.; Peng, C.; Gao, L. Dynamic event-triggered fuzzy control of DC microgrids under FDI attacks and imperfect premise matching. *Int. J. Electr. Power Energy Syst.* **2023**, *147*, 108890. [[CrossRef](#)]
71. Zhang, Y.; Wei, L.; Fu, W.; Chen, X.; Hu, S. Secondary frequency control strategy considering DoS attacks for MTDC system. *Electr. Power Syst. Res.* **2023**, *214*, 108888. [[CrossRef](#)]

Disclaimer/Publisher’s Note: The statements, opinions and data contained in all publications are solely those of the individual author(s) and contributor(s) and not of MDPI and/or the editor(s). MDPI and/or the editor(s) disclaim responsibility for any injury to people or property resulting from any ideas, methods, instructions or products referred to in the content.